University of Graz

Institute of Molecular Biosciences - Structural Biology

Master thesis

Structural Investigation of Substrate Binding in Monoglyceride Lipases

Submitted to the Faculty of Natural Sciences at the University of Graz to achieve the degree of

Master of Science

by

Philipp Aschauer

under the supervision of

Dr. Monika Oberer

Graz,

Acknowledgements

First of all I want to thank Dr. Monika Oberer to give me the opportunity to do my master thesis in structural biology. I am also very thank full fur being assigned to the bMGL Project since this project was very fruitful and gave me a perfect start in scientific research. I also want to thank Monika and NAWI Graz for a 6 months scholarship in the "Forschungsbeihilfe" program.

Of course another person to thank is Srinivasan Rengachari for being my mentor during my Master Project and for not losing his patients over my sometimes stupid questions.

I also want to thank Andela Dordić for teaching me how to crystallise proteins while Vasan was in the USA.

My deepest gratitude to my family especially my parents and godfather for their psychological and financial backup. I would never have been able to do this without their support.

Statutory Declaration

I declare that I have authored this thesis independently, that I have not used other than the declared sources/resources, and I have explicitly marked all material which has been quoted either literally or by content from the used sources.

Eidesstattliche Erklärung

Ich versichere, dass ich die eingereichte Arbeit selbständig verfasst, andere als die angegebenen Quellen und Hilfsmittel nicht benutzt und mich auch sonst keiner unerlaubten Hilfsmittel bedient habe. Ich versichere ferner, dass ich diese Arbeit bisher weder im In- noch im Ausland in irgendeiner Form als wissenschaftliche Arbeit vorgelegt habe.

Graz, ...

(Signature, Unterschrift)

Abstract

Monoglyceride lipases (MGLs) are the enzymes that catalyse the last step of lipolysis, namely the breakdown of monoglycerides (MGs) into free fatty acids and glycerol. They are members of the serine hydrolase family and show an α/β hydrolase fold. In mammals MGL beside regulates energy homeostasis and also influences endocannabinoid signalling by breaking down 2-AG. In bacteria, MGLs hydrolyse the short chain monoacylglycerols which are cytotoxic. MGL are conserved across species and are specific for catalysing MG hydrolysis. This thesis is aimed at structural investigation of the binding of MGLs to their substrates to get achieve a better understanding of the link between structure and function of this class of proteins.

In this work, 3D structures of MGL form *Bacillus sp. H257* in free form in complex with substrate analogues and in complex with 1-lauroylglycerol are described. The catalytic triad of this protein is constituted by Ser97, Asp196 and His226; Access of substrate to the active site is mediated by a large substrate binding pocket.

bMGL substrate analogue complex structures present interesting conformational changes in the cap region. The changes occur in the form of a restriction in the substrate entrance tunnel to different extend and the closing of the proposed glycerol exit hole. Closer investigation of these structures reveals Ile 145 to be the residue involved in these conformational changes. Comparing the structures of the bMGL-MG analogue complexes it seems, that the chain length specificity is due to the limited size of the substrate binding pocket. This size restriction causes an unusual conformation in the carbon chains making it less favorable to bind substrates with long chains.

Yju3p has been identified and biochemically characterized to be the yeast ortholog of the human MGL. The enzyme shows a K_m of 260 µM which is comparable to the rat and mouse orthologs. The protein has been crystallised and it diffracts to 2.7 Å. Determination of this structure should give deeper insights into the structure-function relationship and evolution of the MGL family.

Additionally the structural characterization of HctB was subject to this thesis. HctB is a Halogenase derived from the hct gene cluster in *Cyanobacterium lyngbya.* It plays an important role in the synthesis of hectochlorine which influences of actin assembly and is a potential antifungal agent.

Zusammenfassung

Monoglyzerid Lipasen sind Enzyme die den letzten Schritt der Lipolyse katalysieren, wobei sie Monoglyzeride in Glyzerol und freie Fettsäuren spalten. Sie sind Mitglieder der Serinhydrolase Familie und weisen eine α/β Hydrolase Faltung auf. In Säugetieren reguliert MGL, durch seine Rolle im Lipidmetabolismus, den Energiehaushalt; außerdem beeinflusst sie das Endocanabinoidsystem. In Bakterien hydrolisiert MGL kurzkettige Monoglyceride welche ansonsten zytotoxisch wären. Monoglyzerid-Lipasen sind in allen Spezies konserviert und spezifisch für die Hydrolyse von Monoglyzeriden. Diese Arbeit zielt auf die Untersuchung der Bindung von Monoglyzerid-Lipasen zu ihren Substraten ab um besseres Verständnis der Beziehung zwischen Struktur und Funktion dieser Enzyme zu erlangen.

In dieser Arbeit wurden 3D Strukturen der Monoglyzerid Lipase aus *Bacillus sp. H257* in freier Form, in Komplex mit Substratanalogen und in Komplex mit 1-Lauroylglycerol bestimmt. Die katalytische Triade dieses Proteins besteht aus Ser97, Asp196 und His226. Der Zugang des Substrates zum aktiven Zentrum wird durch eine weite Substratbindungstasche gewährleistet.

Die Strukturen der Komplexe von bMGL mit Substratanalogen zeigen interessante Änderungen in der Konformation des Deckelbereichs. Diese Konformationsänderung zeigt sich in Form einer Verengung der Substratbindungstasche und der Glycerolausgansöffnung („glycerol-exit hole“). Nähere Analyse dieser Strukturen zeigt, dass diese Bewegungen von Ile145 durchgeführt werden und eher zufällig zu sein scheinen. Ein Vergleich der Komplexstrukturen zeigt, dass längere Ketten verdreht werden müssen um in der Substratbindungstasche Platz zu finden. Dies weist darauf hin, dass die Spezifität für kürzere Ketten durch das limitierte Fassungsvermögen der Substratbindungstasche hervorgerufen wird.

Yju3p wurde als Ortholog zur menschlichen MGL in Hefe identifiziert. Es weist einen Km Wert von 260 µM auf, was etwa den Werten der orthologen Proteine der Maus und der Ratten entspricht. Das Protein wurde kristallisiert und Streuung bis 2.7 Å wurde erreicht. Die Bestimmung dieser Struktur sollte zu besserem Verständnis der Struktur-Funktion Beziehung und der Evolution der Monoglyzeridlipase führen.

Zusätzlich dazu beschäftigt sich diese Arbeit mit der strukturellen Charakterisierung von HctB. HctB ist eine Halogenase die vom hct Gencluster in *Cyanobacterium lyngbya* codiert wird. Es spielt eine wichtige Rolle bei der Biosynthese von Hectochlorin, welches Einfluss auf die Actinzusammenlagerung hat und antifungale Eigenschaften aufweist.

Content

1. Introduction

1.1. Lipases

Hydrolases are enzymes catalysing the hydrolysis of ester, ether, peptide, glycoside, or anhydride bonds and they represent the third group of EC classifications (e.g. esterases = EC3.1). According to the different substrates used, members of the hydrolases are peptidases, nucleases, phosphatases, glycosidases and esterases.

$$A\text{-}B + H_2O = A\text{-}H + B\text{-}OH$$

Figure 1 General reaction scheme for hydrolases

Lipases are enzymes that catalyse the hydrolysis of ester bonds in lipids, and therefore belong to the family of hydrolases. Lipid hydrolysing enzymes are a subclass of ester hydrolases and can be categorized by the substrates they act upon (including triacylglycerol lipases, carboxyl esterase, cholesterol esterases, phospholipases and lysophospholipases) (1). Lipases have been identified in many organisms throughout all the kingdoms of life; they carry out and regulate many important biological functions such as energy homeostasis, membrane turn-over or signal transduction. Aberrations associated with the function of lipases have been identified as major risk factors in metabolic disorders such as cardiovascular diseases, obesity and cancer (2-5).

1.2. Lipolysis

White adipose tissue serves as the major fat store in mammals. After nutrition intake excess free fatty acids are esterified to triglycerides (TG), to make them chemically more stable. These triglycerides (TGs) are stored in so called lipid droplets in the cytosol of adipocytes. Additionally non-adipocyte cells can store and esterify free fatty acids and hydrolyse them on demand for energy production or lipid synthesis, yet their lipid storage potential is relatively low. Adipocytes can produce free fatty acids in much larger scales and can secret them to supply the whole organism with substrates for energy production (6-9). Lipolysis is a reaction cascade that ultimately converts TGs into three free fatty acids and glycerol respectively.

Lipolysis is carried out by three different enzymes, namely adipose tissue glyceride lipase (ATGL), hormone sensitive lipase (HSL) and mono glyceride lipase (MGL). ATGL catalyses the hydrolysis of a first ester bond converting a triglyceride into a diglyceride and thereby releasing a free fatty acid, HSL cleaves a diglyceride into a monoglyceride (MG) resulting in another a free fatty acid release by hydrolysing an ester bond. Finally MGL converts the monoglyceride into a free fatty acid and glycerol.

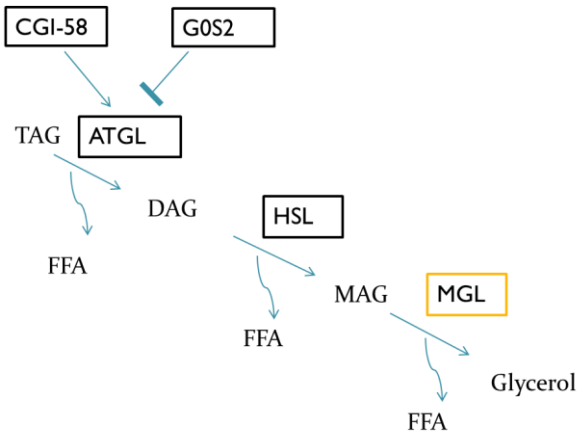

Figure 2 Schematic diagram of lipolysis

1.2.1. ATGL

The role of ATGL in lipolysis became even more evident after reduced lipolysis and excessive lipid storage was observed in ATGL knockout mice (10). The lipid accumulation mainly takes place in oxidative tissue such as muscles and kidney. The tremendous fat accumulation in the muscles of the heart leads to cardiac dysfunction and results in early death (10). Although ATGL is specific for TGs and shows virtually no activity for diglycerides, phospholipids and cholesterol, it also acts as weak acylglycerol transacylase (21, 11). ATGL was identified to contain a patatin-like domain it therefore belongs to a family of proteins called patatin-like phospholipase domain-containing proteins (12). The patatin domain performs non-specific lipid hydrolase activity and possesses a catalytic dyad, composed of the amino acids Ser and Asp. The nucleophile serine is positioned in the classical GXSXG motif and the aspartate in the DXG motif (13). ATGL activity is controlled by two regulatory proteins. CGI-58 has been identified to play a major role in ATGL activation, *in vivo* and *in vitro* (14), G0S2 was shown to selectively inhibit ATGL (15).

1.2.2. HSL

HSL was the first enzyme identified in hormone induced lipid catabolism. HSL shows a broad specificity and catalyses the hydrolysis of TG, diacylglycerol (DG), MG, cholesteryl esters, retinyl esters, and other esters (17). HSL is controlled by two mechanisms, phosphorylation by protein kinases on the one hand and interactions of regulating proteins on the other. One example for these proteins is perilipin (18). Perilipin plays a major role during hormone stimulation of HSL as it mediates the recruitment of HSL to the surface of the lipid droplet upon phosphorylation of perilipin (19,*20*). Hormone sensitive lipase is considered to have two different domains, where the C terminal domain is considered exert catalytic activity and to consist of a α/β-hydrolase core and a regulatory domain harbouring the phosphorylation site (23).

1.2.3. MGL

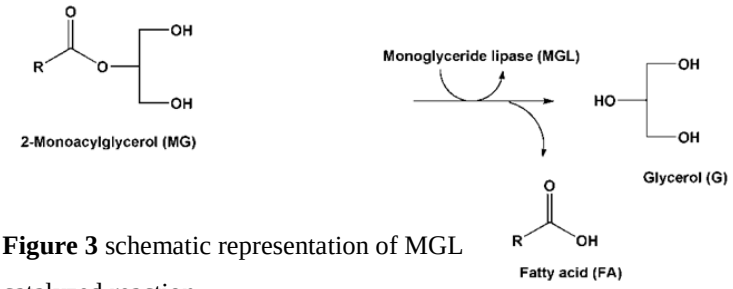

Figure 3 schematic representation of MGL catalyzed reaction

Monoglyceride lipase is the enzyme catalysing the last step of lipolysis, which is the hydrolysis of a MG into a free fatty acid and glycerol (24). MGL is present in all kingdoms of life from eukaryotes i.e. humans, mice and yeast to prokaryotes such as *Mycobacteria* and *Bacillus* species. They carry out different functions based on the physiological demands of their host organisms. In humans for example MGL also catalyses the breakdown of 2-AG in the brain and influences the endocannabinoid system (25). In microbes, MGs are reported to be cytotoxic. As a consequence, MGs are often used as antimicrobial agents in the food industry, therapeutic, and pharmaceutical applications (27-30). Moreover, a role of MGL in the progression of melanoma, human breast, ovarian and colorectal cancer has been identified. Inhibition of MGL activity in these cancers shows a marked suppression of cell proliferation (34, 35).

1.3. The hct cluster

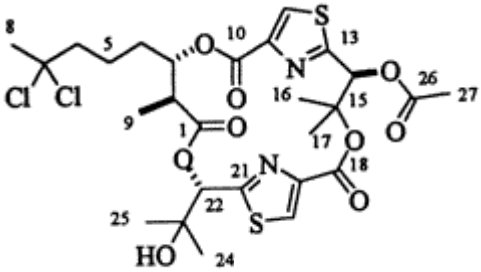

Figure 4 Structure of hectochlorin (**39**)

Hectochlorin is an agent synthesized by cyanobacteria that is expected to have antifungal effects (38) and to interact with actin assembly (39). It was found to be planar and structurally similar to cytoskeleton disrupting proteins such as lyngbyabellins A (39, 40). The hct gene cluster is a region on the chromosome of the *Cyanobacterium lyngbya majuscule*. It encodes for several proteins that are involved in the synthesis of hectochlorin (38). The cluster contains 8 open reading frames spanning 38kb. The 8 proteins resulting from these open reading frames are suspected to have different roles during hectrochlorin synthesis (Table 1).

HctA	acyl-ACP synthetase
HctB	putative halogenase, acylcarrier protein
HctC	Transposase
HctD	polyketide synthase
HctE	nonribosomal peptide synthetase
HctF	nonribosomal peptide synthetase
HctG	cytochrome P450, monooxygenase
Hct H	cytochrome P450, monooxygenase

Table 1 Names and proposed functions of hct gene cluster proteins (38)

1.4. Protein crystallography

1.4.1. Crystallization

One of the key steps towards obtaining X-ray diffraction data and subsequently determining the 3D structure of a protein by crystallography is certainly the crystallization of that protein. This is a very tricky and basically not very well understood procedure, because there are plenty of parameters that influence the crystal growth such as protein concentration, homogeneity of the protein sample, temperature, pH, type of the buffer system, salt concentrations, presence of nucleation cores, type and concentration of additives, etc. There are hundreds of chemicals, which could promote or disturb crystal growth ore disturb it, the difficult part is to find out which of these chemicals help for a particular protein. Another parameter influencing the experiment is the design of the crystallization setup. Common methods are the hanging drop and sitting drop vapour diffusion method (41).

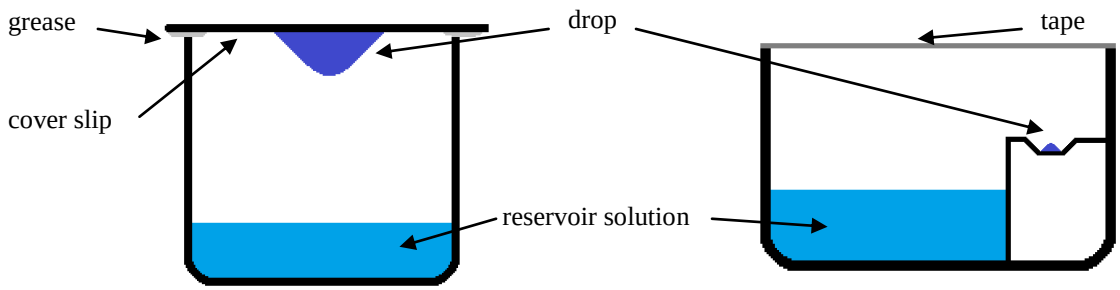

Figure 5 Vapor diffusion methods left) hanging drop right) sitting drop

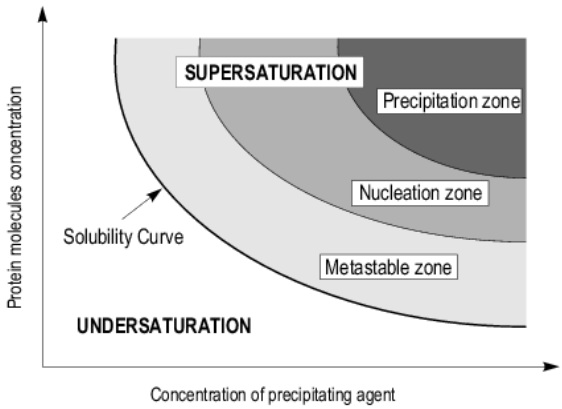

Figure 6 Phase diagram for protein crystallization (**42**)

The hanging drop method uses a cover slip positioned over a reservoir containing the crystallization condition. A drop composed of crystallization condition and protein solution is positioned on this plate in way so it hangs inside the chamber. The whole setup is sealed with vacuum

grease to protect the setup from drying out. The sitting drop setup has a small pedestal, where the drop is positioned and the chamber is sealed with a tape but the overall principal is same as hanging drop method (Figure 5). The idea behind vapour diffusion experiments is to have the protein in an under saturated state at the beginning of the experiment. The setup is then allowed to equilibrate, which means water evaporates form the drop and the reservoir, till the chamber is saturated with humidity. As the equilibrium is formed, the protein and the precipitant concentrations in the drop are rising, shifting the drop solution from the under saturated zone into the nucleation zone (Figure 6). In the nucleation zone nucleation cores are formed, this process is consuming protein shifting the solution to the metastable zone. Here no new nucleation cores are formed but the crystals are free to grow to the point where the solution hits the intersection to the under saturated zone.

Sparse matrix screens were developed, based on statistics of already crystallised proteins, and contain chemicals that where observed to lead to crystallization most frequently. These screens (e.g. JCSG+ or Morpheus, Molecular Dimensions, Suffolk, UK) reduce the problem that it is impossible to know which precipitant, buffers, salts or additives to use at the beginning of an experiment.

1.4.2. X-ray diffraction analysis

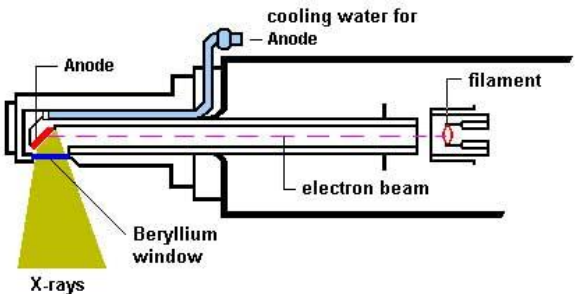

Figure 8 x-ray tube with side window (**43**)

Once a crystal is obtained from a crystallization setup, the crystal needs to be exposed to X-ray. First to make sure the crystal under investigation is a protein and not a salt crystal, later on (often after the crystal was optimized) to collect a data set in order to determine the 3D structure. This is done by exposing the crystal to X-ray radiation and interpreting the resulting diffraction patterns. There are two major types of X-ray sources: One way to create X-ray radiation is to bombard an anode made of a heavy metal (e.g.

Figure 7 SLS synchrotron facility at PSI (Villigen, CH) (**44**)

copper) with electrons created by heating a tungsten filament. This method is used in X-ray tubes (Figure 8) or rotating anodes. Two types of radiation are occurring when the electron passes through anode material. The first type is so-called bremsstrahlung which results from acceleration/deceleration of electrons in the strong electric fields of atomic nuclei. In this case the electron gets decelerated and emits part of its energy as radiation yielding a continuous spectrum. The second type is characteristic radiation. It is created, when the electron knocks another electron out of the anode material. The resulting empty space is filled by an electron descending from a higher shell and emitting the energy difference as radiation. X-ray diffraction analysis of protein crystals uses exclusively characteristic radiation as for example Cu Kα (an electron in copper transitions from the L shell to the K shell). Another method to create radiation is to accelerate a charged particle (e.g. electron) in a circular manner by deflecting it with electromagnets. The resulting radiation is called synchrotron radiation and ranges over the whole spectrum (Figure 7).

Once a good enough crystal is obtained and exposed to X-ray radiation, a diffraction pattern can be observed, caused by the electrons of the protein diffracting the X-ray beam.

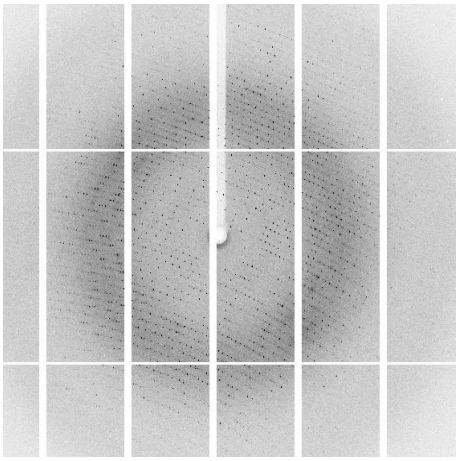

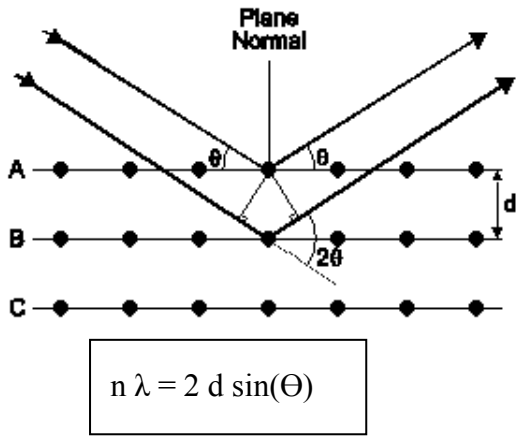

Figure 9 left) example for protein diffraction (chapter 3.7.5.), right) Braggs law (**45**)

Since proteins are big molecules and the images are taken in reciprocal space an important characteristic of protein diffraction is that low resolution reflections are observed (in the middle of the image). Bragg´s law determines the rules that are necessary for positive interference between the planes in the crystal and therefore the requirements to create a reflection on the detector. The distance between the plains (d) times the sinus of the angle with which the x-ray hits these plans (Θ) times 2 needs to be an integer multiple of the wave

length. If this is fulfilled positive interaction occurs and the reflections can be observed, if not the destructive interference extinguishes the scattered X-ray (Figure 9).

a) $$I(\vec{R}) = F(\vec{R})F^{*}(\vec{R}) = \left|F(\vec{R})\right|^{2} \qquad \left|F(\vec{R})\right| = \sqrt{I(\vec{R})}$$

b) $$\rho(\vec{r}) = FT^{-1}\left(F(\vec{R})\right) = \int\int\int F(\vec{R})e^{-2\pi i\vec{r}\vec{R}}d^{3}\vec{R}$$

Figure 10 Relationships between measured reflections and electrondensity

One big problem in X-ray crystallography is the link between the intensities we can measure from our images (I(R)) and the structure factor F(R) which is necessary to calculate the electron density ρ(r). As shown in Figure 10a) we cannot really obtain the structure factor F(R) but only its absolute value. Since F(R) is a vector, this means we have the length of the vector but lose information of its phase (the direction in which the vector points). Unfortunately the phase is crucial to calculate the position of the electron densities, thus it is inevitable to retrieve the information of the phase. This is called the crystallographic phase problem.

One of the many approaches to solve the phase problem is molecular replacement (MR). This method requires a 3D model that is structurally similar to the protein of which the phase problem should be solved. If such a model is available (e.g. from experimentally determined structures) Patterson functions (Fourier function of the squares of the structure factors) of this model and of the measured data set is calculated. To calculate a Patterson function the phases are not needed. A drawback is that the Patterson function does not give absolute atom positions, but the positions of the atoms relative to each other. The model is rotated and translated, until the two Patterson functions fit as good as possible. Now the phase information can be calculated from the atomic coordinates of the model (Figure 10b)). Since the phases for the data set are calculated from the atom positions of the model, a wrong model can result in wrong phases and un-interpretable electron density.

2. Project MGL

All the work on MGLs described in this chapter was done in collaboration with Srinivasan Rengachari.

2.1. Introduction

2.1.1. bMGL and YJU3

The enzyme referred to as bMGL in this thesis is the monoglyceride lipase found in thermophilic *Bacillus sp. H257*. Since MGs are toxic for bacteria, MGL plays a major role in their survival. Interestingly bMGL shares only 17% sequence identity with MGL from human although they catalyse the same reaction. bMGL has been found to be highly specific for MGs, and shows the highest activity for 1-lauroyl glycerol (1-LG) (36).

Substrate	Specific activity (mmol/h*mg)
1- monocapryloyl glycerol ($C_{8:0}$)	6.8
1-monolauroyl glycerol ($C_{12:0}$)	7.2
1-monomyristoyl glycerol ($C_{14:0}$)	6.1
1-monoparmitoylglycerol ($C_{16:0}$)	4.5
1-monostearoylglycerol ($C_{18:0}$)	3.2
1-monooleoylglycerol($C_{18:1}$)	4.1

Table 2 bMGL substrate specificity

Recently the 3D structure of bMGL in its free form and in complex with PMSF has been determined in our group by X-ray crystallography (31). The 250 amino acid protein shows a minimal α/β-hydrolase fold with Ser97, Asp196 and His226 as the members of the catalytic triad. It is called minimal α/β-hydrolase fold because it is missing the N terminal β-strand compared to a canonical α/β-hydrolase fold. In addition to the core region building the α/β-hydrolase fold bMGL also contains a flexible cap region that is built up by a small α-helix (residues 127-130) and two short antiparallel β-strands (residues 141-143, 161-163) connected by a loop region (Figure 12).

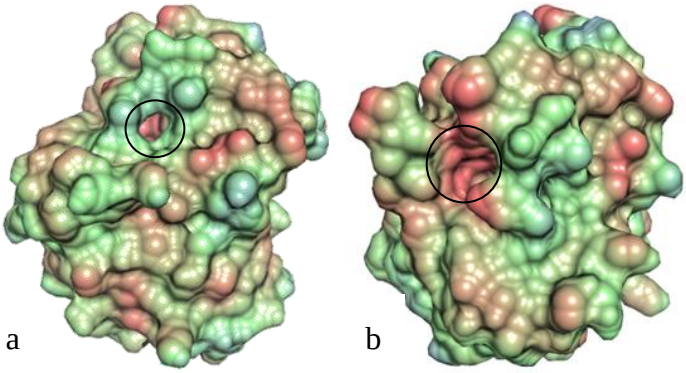

Figure 11 a) proposed glycerol exit hole, b) substrate entrance channel. (**31**)

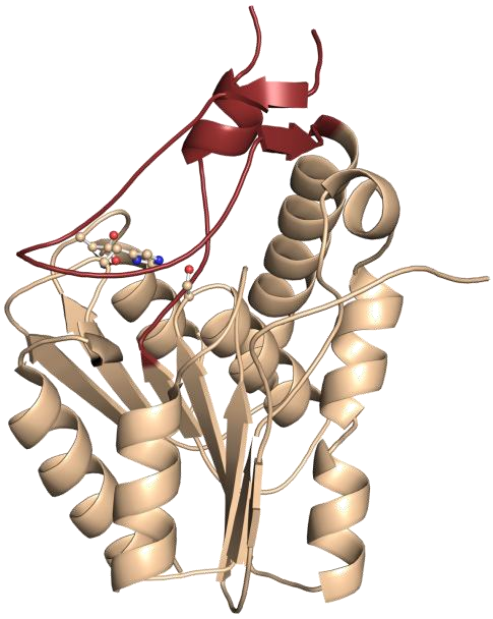

Figure 12 bMGL structure wheat-brown=core region red=cap (**31**)

The active centre (catalytic triad) lies at the bottom of a ~22Å deep channel, that is coated with hydrophobic residues; it therefore separates the active centre from the polar environment (Figure 11b). The bottom of this channel harbouring the catalytic triad shows a polar nature. The substrate entrance channel is flanked by a smaller hydrophilic hole, which is expected to be an exit hole for the glycerol emerging from the hydrolysis of a MG (Figure 11a).

YJU3 has been identified to be the functional orthologous of monoglyceride lipase in *Saccharomyces cerevisiae*. It consists of 313 amino acids and shows 24% sequence identity with human MGL (32, 33). Closer investigation of this protein might contribute to a more detailed understanding of the evolution of MGLs. However the 3D structure of this protein is still unknown.

2.1.2. Covalently binding substrate analogues

In order to study interactions between bMGL and its substrates we use covalently binding analogues of MGs. Nitro phenol esters of alkyl phosphonic acids are known to carry out a nucleophilic substitution reaction with serine hydrolases and therefore stall the catalytic activity by forming an irreversible covalent bond to the serine in the active site (37). These analogues are perfect for our purposes, because the covalent binding prevents the substrate from being cleaved by the enzyme and also from escaping the substrate binding pocket, giving us the opportunity to observe a freeze frame picture of the interactions between substrate analogue and protein. The substrate analogues were synthesized with different chain length and are referred to as C_{12}, C_{14} and C_{16} according to the length of their carbon chains.

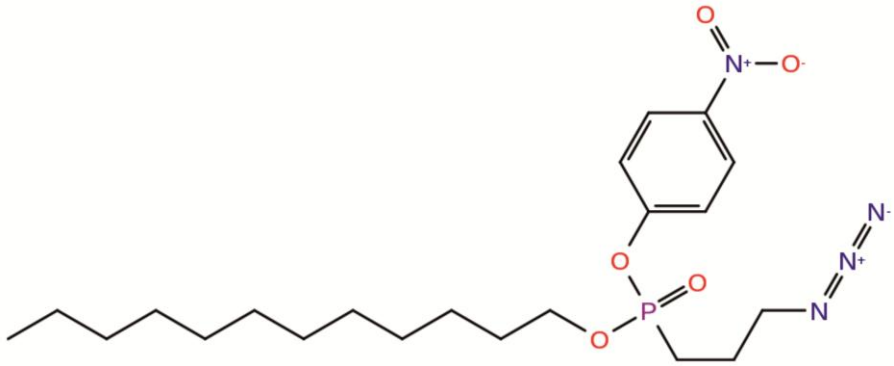

Figure 13 Covalently binding substrate analogue with a 12 carbons long chain

Since the positions of C1 and C2 in a real MG are occupied by phosphor and oxygen in our substrate analogues, the analogue with a chain of 12 carbons (C_{12}) would actually correspond to MG with a 14 carbon long chain.

2.2 Methods

2.2.1 Mutations

All point mutations were done according to the following protocol:

Content	**Forward reaction**	**Reverse reaction**
5x GC buffer	5.00µl	5.00 µl

Template (100ng/µl)	0.50 µl	0.50 µl
Primer (20pm/µl)	2.00 µl (Fwd Primer)	2.00 µl (Rev Primer)
dNTP (10mM of each dNTP)	1.00 µl	1.00 µl
H_2O (nuclease free)	15.75 µl	15.75 µl
Phusion polymerase(2000 U/ml)	0.25 µl	0.25 µl

Table 3: Reaction mixture for PCR

All point mutations were done using a pET28a(+) vector (Novagen, Merck, Whitehouse Station, USA) with the gene for the monoglyceride lipase from *Bacillus* sp. H257 between the NdeI and XhoI sites as template (31).

These reactions were carried out using an Eppendorf mastercylcer (Eppendorf AG, Hamburg Germany). Initial denaturation was done at 98°C for one minute. The cycle consisted of a denaturation phase (for 50sec at 98°C) an annealing phase (40 sec at 63°C) and an elongation phase (7min at 72°C). A final elongation was allowed to take place for 10min at 72°C.

After the first 5 cycles the forward and reverse reactions were mixed together and 15 more cycles were executed.

Afterwards 2.5µL DpnI (20000U/ml) were added to the resulting PCR product and incubated at 37°C for 3h. The DpnI digested PCR product was then transformed into Top 10 cells as described in chapter 3.2.

<u>Primers used:</u> (Invitrogen Carlsbad, California, USA)

Mutant	**Primers**
I145G	Fwd: GCC GAG GTA TCT GGA TTC GGG CGG TTC GGA CTT G Rev: CAA GTC CGA ACC GCC CGA ATC CAG ATA CCT CGG C
I145S	Fwd: GCC GAG GTA TCT GGA TTC GAG CGG TTC GGA CTT G Rev: CAA GTC CGA ACC GCT CGA ATC CAG ATA CCT CGG C

D196N	Fwd: TTT TGT CTC CGA CGA AAA TCA CGT CGT GCC GC Rev: GCG GCA CGA CGT GAT TTT CGT CGG AGA CAA AA

Table 4: Primers used to create bMGL mutants

2.2.2 Transformations

2.2.2.1 bMGL wt

pET28a(+) (Novagen, Merck, Whitehouse Station, USA) vector with the gene for the monoglyceride lipase from *Bacillus Sp. H257* between the NdeI and XhoI sites (90ng/µl) was mixed with a 200µl chemically competent (47) *E.coli* cells of the strain BL21 (DE3) and incubated on ice for 30min. Subsequently the cell/plasmid mixture was delivered a heat shock for 45 seconds on 42°C. After resting the cells on ice for 2 minutes, 800µL Luria-Bertani broth was added. Then the cells were allowed to grow for 45 min at 37°C and centrifuged for 1 minute with 3,3g (Centrifuge 5415R, Eppendorf AG, Hamburg Germany). 800µL of the resulting supernatant were discarded and the pellet was resuspended in the rest of the supernatant. This suspension was plated on LB-Agar plate with kanamycin (40µg/ml) and incubated over night at 37°C.

2.2.2.2 YJU3 L171S

1µL pPro Ex Htb vector (Invitrogen, Carlsbad, California, USA) with the gene for the YJU3 L171S mutant cloned between the BamHI and EcoRI sites (150ng/µl) was mixed with a 200µl culture competent (47) *E.coli* cells of the strain (BL21 DE3) and kept on ice for 30min (32) Subsequently the cell/plasmid mixture was treated with a heat shock for 45 seconds at 42°C.After a 2 minute resting period on ice the culture was mixed with 800µL Luria-Bertani broth. Now the cells were allowed to grow for 45 min at 37°C and centrifuged for 1 minute with 3,3g (Centrifuge 5415R, Eppendorf AG, Hamburg Germany). 800µL of the resulting supernatant were discarded and the pellet was resuspended in the rest of the supernatant. This suspension was plated on LB-Agar plate with ampicillin (100µg/ml) and incubated overnight at 37°C.

2.2.2.3. bMGL D196N

10µL of PCR product (described in chapter 3.1) was mixed with a 200µL culture *E.coli* cells of the cloning strain Top 10 (47) and incubated on ice for 30min. Subsequently the cell/plasmid mixture was delivered a heat shock by putting it at 42°C for 45 seconds. Afterwards the mixture was put on ice for 2 minutes and then mixed with 800µL Luria-Bertani broth. Now the cells were allowed to grow for 45 min at 37°C and centrifuged for 1 minute 3.3g (Centrifuge 5415R, Eppendorf AG, Hamburg Germany). 800µL of the resulting supernatant were discarded and the pellet was resuspended in the rest of the supernatant. This suspension was put on an LB-Agar plate with Kanamycin (40µg/ml) and incubated over night at 37°C.

The next day an overnight culture was prepared by inoculating a single colony of the calls transformed the day before into 10ml Luria-Bertani broth containing 40µg/ml Kanamycin.

This overnight culture was centrifuged 10min 3220g(Centrifuge 5180R, Eppendorf AG, Hamburg Germany) and after a isolating the plasmids using a Miniprep Kit (QIAprep Spin Miniprep Kit(250), QIAGEN GmbH, 40724 Hilden, Germany) the plasmid was sent for sequencing (LGC Genomics GmbH, Berlin, Germany)

1µl of this plasmid was mixed with a 200µL culture *E.coli* cell culture of the strain BL21 DE3 and kept on ice for 30min. Subsequently the cell/plasmid mixture was delivered a heat shock by putting it on 45 seconds on 42°C. After that the mixture was put on ice for 2 minutes and then mixed with 800µL Luria-Bertani broth. Now the cells were allowed to grow for 45 min at 37°C and centrifuged for 1 minute with 3.3g (Centrifuge 5415R, Eppendorf AG, Hamburg Germany). 800µL of the resulting supernatant were discarded and the pellet was resuspended in the rest of the supernatant. This suspension was plated on a LB-Agar plate with kanamycin and incubated over night at 37°C.

2.2.2.4. bMGL I145G & I145S

The transformation of the I145 mutants into Ecoli Top10 cells, the plasmid isolation and the transformation of this plasmid into Ecoli BL21 (DE3) cells were done the same way as for the D196N mutant (chapter 2.2.3.).

2.2.3. Protein Expression

2.2.3.1. bMGL

An *E.coli* BL21 (DE3) colony (chapter 3.2.1.) was inoculated into sterile LB broth with 40µg/ml Kanamycin and incubated at 37°C and 180rpm overnight. The next day 10ml of this overnight culture were inoculated into 12 flasks containing 500ml sterile LB broth with 40µg/ml Kanamycin. The main cultures were grown at 37°C and 180rpm till they reached an optical density (600nm) of 0.5. At this point gene expression was induced by adding 1M IPTG to achieve a final concentration of 0,5mmol/l. After additional incubation at 37°C and 180rpm for 4 hours, the cells where harvested by centrifuging the cell-suspension for 10min at 2831g (Avanti J-26XP centrifuge, rotor JA 10, Beckman-Coulter GmbH, 47807 Krefeld, Germany). The resulting pellet was divided into 2 aliquots, each of this aliquots was resuspended in 50ml 0.9%NaCl solution and again centrifuged for 30 min at 3220g (Centrifuge 5180R, Eppendorf AG, Hamburg Germany). The pellets were stored at -20°C

The bMGL D196N, I145S and I145G mutants were overexpressed following the same protocol as the wild type protein, using the cells described in chapter 2.2.2.1 bMGL wt.

2.2.3.2. YJU3 L171S

An *E.coli* BL21 (DE3) colony (chapter 3.2.3.) was inoculated into 120ml sterile LB broth with 100µg/ml ampicillin and incubated at 37°C and 180rpm overnight. This overnight culture was inoculated into 12 flasks containing 500ml sterile LB media with 100µg/ml ampicillin each. The main cultures were grown at 37°C and 180rpm till they reached an optical density (600nm) of 0.8. At this point overexpression was induced by adding 1M IPTG to achieve a final concentration of 0.5mmol/l. After additional incubation at 37°C and 180rpm for 4 hours, the cells where harvested by centrifuging the cell-suspension for 10min at 2831g (Avanti J-26XP centrifuge, rotor JA10, Beckman-Coulter GmbH, 47807 Krefeld, Germany). The resulting pellet was divided into 2 aliquot. Each aliquot was resuspended in 50ml 0.9%NaCl solution and again centrifuged for 30 min with 3220g (Centrifuge 5180R, Eppendorf AG, Hamburg Germany). The pellets were stored at -20°C.

2.2.4. Purification

For all affinity purifications gel samples of the flow through from the loading, washing and elution fraction were collected to monitor the purity of the protein by SDS polyacrylamide gel electrophoresis. The electrophoresis was carried out using a Mini PROTEAN^{R} Tetra Cell (Bio-Rad Laboratories Ltd.**,** Hemel Hempstead, UK) following the protocol in chapter **Fehler! Verweisquelle konnte nicht gefunden werden.**. Unstained protein (Fermentas GmbH, St. Leon-Rot, Germany) was used for all the SDS polyacrylamide electrophoreses. The gel filtration standard from BIO-RAD (Bio-Rad Laboratories Ltd., Hemel Hempstead, UK) was used to determine the oligomeric state of the size exclusion fractions. The electrophoresis was carried out using a Mini PROTEANR Tetra Cell (Bio-Rad Laboratories Ltd., Hemel Hempstead, UK). To make the proteins visible the gel was stained for 10 min with a solution of 0.5% Commassie R brilliant blue, 50% ethanol and 10% acetic acid and then destained with hot water over night.

2.2.4.1. bMGL

bMGL wild type and the D196N, I145S and I145G mutants were purified the same way, with the same solutions but with different Ni-NTA columns.

After thawing a cell pellet (described in chapter 3.3.1.), it was resuspended in ca. 50ml lysis buffer (20mM Tris pH 8.0, 100mM NaCl;), homogenized (ULTRA TURRAX T25, IKA®-Werke GmbH & CO. KG, 79219 Staufen, Germany) and sonicated (SONOPLUS HD 2070, BANDELIN electronic GmbH & Co. KG, 12207 Berlin, Germany) for 12.5min with the following settings: Cycle=5, Power=50%. The resulting suspension was centrifuged (Avanti J-26XP centrifuge, rotor JA 25.50, Beckman-Coulter GmbH, 47807 Krefeld, Germany) for 30min at 23708g and 4°C. The supernatant was filtered through a 0.45µm syringe filter. This filtered supernatant was loaded onto a self-packed Ni-NTA resin (QIAGEN GmbH, 40724 Hilden, Germany), it was then washed with 10-15 column volumes washing buffer to wash of the impurities (100mM NaCl; 20mM Tris pH 7.5; 40mM imidazol) and the protein was eluted with 5 column volumes elution buffer (20mM Tris pH 7.5, 100mM NaCl, 250mM imidazol). This elution fraction was dialyzed against 2L dialysis buffer (20mM Tris pH 7.5, 100mM NaCl) overnight, using a 12-14kDa cutoff dialysis bag (Spectra/Por, Spectrum Laboratories,

Inc.). The following day the dialysed sample was concentration to approximately 10ml and a size exclusion chromatography was performed using 250ml Superdex 200 resin (Pharmacia XK 26, GE Healthcare, Solingen, Germany) at a flow rate of 2ml/min; 2ml fractions were collected between 70ml-250ml (the buffer was the same as the dialysis buffer). Subsequently the monomer fractions were pooled, concentrated to approximately 25mg/ml, shock frozen with liquid nitrogen and stored at -80 °C.

2.2.4.2. YJU3 L171S

After thawing a cell pellet (described in chapter 3.3.2.), it was resuspended in ca. 50ml lysis buffer (20mM Tris pH 8.0, 100mM NaCl), homogenized (ULTRA TURRAX T25, IKA®-Werke GmbH & CO. KG, 79219 Staufen, Germany) and sonicated (SONOPLUS HD 2070, BANDELIN electronic GmbH & Co. KG, 12207 Berlin, Germany) for 12.5min with the following settings: Cycle=5, Power=50%. The resulting suspension was centrifuged (Avanti J-26XP centrifuge, rotor JA 25.50, Beckman-Coulter GmbH, 47807 Krefeld, Germany) for 30min at 23708g and 4°C. The supernatant was filtered through a 0.45µm syringe filter. This filtered supernatant was loaded onto a self-packed Ni-NTA (QIAGEN GmbH, 40724 Hilden, Germany) resin, it was then washed with 10-15 column volumes washing buffer to wash off the impurities(20mM Tris pH 8.0, 100mM NaCl, 40mM imidazol) and the protein was eluted with 5 column volumes elution buffer (20mM Tris pH 8.0, 100mM NaCl, 250mM imidazol, 5% Glycerol). This elution fraction was dialysed against 2l dialysis buffer (20mM Tris pH 8.0, 100mM NaCl, 5% Glycerol, 1mM DTT, 1mM EDTA) overnight using a 12-14kDa cut off dialysis bag (Spectra/Por, Spectrum Laboratories, Inc.). That following day the dialysed sample was concentrated to approximately 10ml and a size exclusion chromatography was performed using a 250ml Superdex 200 resin (Pharmacia XK 26, GE Healthcare, Solingen, Germany) column using a flow rate of 2ml/min; 2ml fractions were collected between 70ml-250ml (the buffer was the same as the dialysis buffer).

Subsequently the monomer fractions were pooled, concentrated to approximately 15mg/ml, shock frozen with liquid nitrogen and stored at -80 °C.

2.2.3. Crystallization

All hanging drop plates were set up by hand; all sitting drop plates were set up using an Oryx8 crystallization robot (Douglas Instruments Ltd, Berkshire, United Kingdom). The typical drop sizes were 1µl for sitting drop, 4µl for hanging drop and 5 µl for hanging drop experiments with seeding. The reservoir volumes were 30µl for sitting drop and 500µl for hanging drop.

2.2.3.1. bMGL C_{12} complex

0.9 mM (~26mg/ml) of bMGL was mixed with 50 mg/ml of C_{12} ligand dissolved in DMSO to achieve a final concentration of 4.5 mM ligand (1:5 ratio). Crystallization trials were performed using sitting drop vapour diffusion method with equal volumes of bMGL-C_{12} complex and the Morpheus screen (Molecular Dimensions, Suffolk, UK) reservoir solution containing 0.1 M MES/imidazole pH 6.5, 12.5% w/v PEG 1000, 12.5% w/v PEG 3350, 12.5% v/v MPD and 0.12 M alcohol mix. Well diffracting crystals were obtained from the drop within two weeks without further optimization and no additional cryo-protectant was used for flash cooling the crystals in liquid nitrogen **(Figure 24)**.

2.2.3.2. bMGL C_{14} complex

0.9 mM (~26mg/ml) of bMGL was mixed with 50 mg/ml C_{14} ligand, dissolved in 99% EtOH to achieve a final concentration of 4.5mM ligand (1:5 ratio). The protein ligand mixture was stirred for 1 hour at 4° C and the mixture was spun down at 16.1g for 10 minutes.

Crystallization trials were set up using sitting drop vapour diffusion method with equal volumes of free bMGL complex and reservoir solutions of commercially available screens. Initial crystals were obtained from the condition containing, 0,1M citric acid pH 5.5 and 20% w/v PEG3000 (condition A2 from JCSG+ screen) (Figure 25). These crystals showed highly mosaic diffraction pattern, therefore they were improved by optimizing the precipitant concentration versus the pH value from which non-diffracting but initially more promising crystals were obtained in a solution of 16% w/v PEG3350 and 0.1M citric acid pH 5.8 (Figure 26). Further optimization of this condition with the bMGL C_{14} complex gave again crystals in the same condition (Figure 27). These crystals were optimized using the hanging drop

method; well diffracting crystals (1.85Å) were obtained after two weeks from the drop containing 0.1M citric acid pH 5.2 and 18% PEG 3350 (Figure 28).

2.2.3.3. free bMGL in C_{14} complex condition

bMGL free enzyme of ~25 mg/ml was used to set up crystallization trials using hanging drop vapour diffusion method. The crystals of dataset quality were obtained after 2 weeks from the same crystallization conditions as described for the bMGL - C_{14} ligand complex (Figure 31).

2.2.3.4. bMGL C_{16} complex

0.9 mM (~26 mg/ml) of bMGL was mixed with 50 mg/ml C_{16} ligand**,** dissolved in 99% EtOH to achieve a final concentration of 4.5mM (1:5 ratio). The protein ligand mixture was stirred for 1 hour at 4° C and the mixture was spun down at 16.1g for 10 min. Optimization of this condition using the hanging drop method, yielded well diffracting crystals within 10 days in a condition containing 0.1M citric acid pH 5.0 and 22% PEG 3350 (Figure 32).

2.2.3.5. bMGL D196N in complex with 1-LG

0.9 mM of bMGLD196N was mixed with 1-LG (140mM) or 1-OG (180mM) dissolved in 99% EtOH to achieve a final protein/ligand ratio of 1:5. The protein ligand mixture was stirred for 1 hour at 4° C and the mixture was spun down at 16.1g for 10 min.

0.9mM of bMGLD196N mutant was used to set up a Morpheus screen (Molecular Dimensions, Suffolk, UK) using the sitting drop method and equal volumes of protein and reservoir solution. Initial crystals were obtained in Morpheus condition A4 containing 12.5% w/v PEG1000, 12,5% w/v PEG3350, 12,5% v/v MPD, 0,06M divalent cation mix 0,1M MES/Imidazol pH 6.5 (Figure 34). These crystals were used to prepare a seeding stock by mixing the drop with 50 µl original Morpheus A4 condition, and vortexing with a seed bead (HR2-320, Hampton research, California, USA).

This seeding stock was used to set up a JCSG+ screen (Molecular Dimension limited, Suffolk, United Kingdom) by mixing 0.4µl bMGLD196N (0.94mmol/ml) with 0.4µl condition and 0.2 µl seeding stock diluted 1:1000. Promising crystals were obtained in the JCSG+ condition H12 containing 45% v/v MPD, 0.3M ammonium acetate and 0.1M HEPES pH7.5 (Figure 35). Optimizing of the precipitant concentration versus the pH value yielded a crystal

diffracting to 8Å. The condition contained 0.4µl bMGLD196N 1-OG complex (0.90mmol/ml) with 0.2µl seeding stock 1:1000 diluted and 0.4µl condition containing 54% v/v MPD and 0.1M HEPES pH 6.8 (Figure 36). Subsequently this crystal was optimized using the hanging drop method. The crystal suitable for collection of a complete dataset was obtained within 2 month mixing 0.4µl bMGLD196N 1LGcomplex with 0.2µl seeding stock diluted 1:1000 and 0.4µl condition containing 56% v/v MPD 0.1M HEPES pH 6.9. These crystals diffracted to 1.85Å (Figure 37).

2.2.3.6. bMGL I145S &I145G

Initial crystallization setups were performed, to crystalize these mutants in the optimized JCSG+ condition were the bMGL C_{14} complex was crystalized in (the reason for this experiment is explained in chapter 2.4.2. Conformational change). Dataset quality crystals were not obtained yet.

2.2.3.7. YJU3 L171S

The initial crystal was obtained from experiments performed by Christian Sturm; this was achieved by setting up a Morpheus screen (Molecular Dimensions, Suffolk, UK) with 0.42mM (~16mg/ml) YJU3 L171S using sitting drop. The condition for this crystal was Morpheus C5 containing 10% w/v PEG 20000, 20% w/v PEGMME 550, 0.09M NPS mix and 0.1M MOPS/HEPES pH 7.5. (Figure 39).

This drop was used to make a seeding stock by mixing it with 50µl original Morpheus C5 condition and vortexed with a seed bead (HR2-320, Hampton research, California, USA).

Again a Morpheus screen was set up by mixing 0.4µl YJU3L171S (0.35mM) with 0.2µl seeding stock diluted 1:100 and 0.4µl condition. A crystal diffracting to 9Å was obtained from condition C9 with 10% w/v PEG 20000, 20% w/v PEGMME 550, 0.09M NPS mix and 0.1M Bicine/Trizma pH 8.5 (Figure 40). Optimization using a pH versus precipitant matrix gave a crystal diffracting to 3.5Å in a condition containing 10% w/v PEG 20000, 20% w/v PEGMME 550, 0.09M NPS mix and 0.1M Bicine/Trizma pH 8.9 (Figure 42). Further hanging drop optimization gave a crystal diffracting to 2.5Å at the SLS micro focus beam line PSXIII by mixing 2µl YJU3L171S (0,36mM) with 1µl seeding stock 100 and 2µl reservoir

solution containing 10% w/v PEG 20000, 20% w/v PEGMME 550, 0.09M NPS mix and 0.1M Bicine/Trizma pH 8.7 (Figure 41).

2.2.4. Structure determination

2.2.4.1. X-ray diffraction

All crystals (see in chapter 2.3.2 Crystallisation) were cryo-cooled in liquid nitrogen without usage of cry protection. Afterwards they were measured using a Microstar (Bruker, Karlsruhe, Germany) X-ray source with a Mar 345 detector (Marresearch GmbH, Norderstedt, Germany) to determine if they are salt and to see if they show protein diffraction. The best crystals were taken to synchrotron facilities to collect datasets using X-ray beams of very high intensities.

Crystal	Synchrotron facility/beam line
bMGL-C_{12} complex (Figure 24)	DESY (Hamburg, Germany)/X13
bMGL-C_{14} complex (Figure 28)	SLS (Villigen, Switzerland)/PXIII-X06DA
Free bMGL in C_{14} complex condition (Figure 31)	ELETTRA (Trieste, Italy)/XRD1
bMGL-C_{16} complex (Figure 32)	ESRF (Grenoble, France)
bMGL D196N in complex with 1-LG (Figure 37)	SLS (Villigen, Switzerland)/PXIII-X06DA
YJU3 L171S (Figure 41)	SLS (Villigen, Swtizerland)/PXI-X06DA (micro focus)

Table 5 Crystals for which datasets were collected at different synchrotrons.

2.2.4.2. Data processing and refinement

All the Ligands were created with the program MAESTRO (Maestro, version 9.3, Schrödinger, LLC, New York, NY, 2012). These models were used as inputs for PHENIX.elbow creating cif library files containing the bond and angle restrains.

2.2.4.2.1. bMGL-wt

The bMGL-C_{14} (1.85Å), bMGLC_{16} (2.2Å) ligand complex datasets and the bMGL free form in C_{14} condition were indexed and integrated using XDS, the bMGL-C_{12} (1.7 Å) was indexed and integrated (2.5 Å) using iMosflm (Leslie, 1992). The scaling of all bMGL wt datasets was done using Scala (Leslie, 1992; Evans, 2006). Molecular replacement for the bMGL-C_{12} complex, the bMGL-C_{16} complex and free bMGL in C_{14} condition was done using Phaser (McCoy et al, 2007); for the bMGL-C_{14} complex the Balbes server (Long et al, 2008) was used to solve the phase problem. The free bMGL structure solved by Srinivasan Rengachari (31(PDB code 3RM3)) was used as model for molecular replacement. In case of the bMGL-C_{14} complex the model building was performed using Arp/warp (Perrakis et al, 1999) . The bMGL-C_{12} and bMGL-C_{14} complex structures were subjected to rigid body and restrained refinement cycles using the program REFMAC5 followed by several iterative rounds of refinement using PHENIX (Murshudov et al, 1997; (Adams et al, 2011)). The free bMGL in C_{14} condition and the bMGL-C_{16} complex were entirely refined with PHENIX (Murshudov et al, 1997; (Adams et al, 2011)).There, water molecules were added and the weights for the X-ray/stereochemistry and X-ray/ADP were optimized resulting in the lowest Rfree value. B-factors of the atoms were refined anisotropic. COOT was used to manually adjust and monitor the structure and the solvent. The MolProbity server was used to validate the model (Chen et al, 2010).

2.2.4.2.5. bMGL D196N 1-LG complex

For the D196N-1LG complex 2 datasets were recorded, one low resolution dataset (3.14Å) and one high resolution data set (1.62Å). These data sets were indexed and integrated using iMosflm (Leslie, 1992;) merged in Pointless and scaled using Scala; (Evans, 2006), where the

data was cut at 1.85Å. The phase problem was solved by molecular replacement, using bMGL free form structure with open conformation as model (PDB code 3RLI) (31). Rigid body refinement and initial refinement was carried out using Refmac5 (Vagin, AA,2004), further refinement was performed with PHENIX (Adams et al, 2011). COOT was used for manually adjustment of the model and for the initial evaluation. The structure was further refined by adjusting solvent and MPD molecules and by fitting the ligand. The R factors came down to final values of Rwork = 0.1567 and Rfree = 0.1736. Residue Ile145 in chain D was the sole Ramachandran outlier (Ile 145).

2.2.4.2.6. YJU3 L171S

Although diffracting crystals and a 2.7Å data set were obtained, the phase problem for YJU3 L171S could not be solved yet. In order to solve the phase problem either a better model for molecular replacement or a different method for solving the phase problem would be needed.

2.3. Results

2.3.1. Purification

Unstained protein (Fermentas GmbH, St. Leon-Rot, Germany) was used for all the SDS polyacrylamide electrophoreses. The gel filtration standard by BIO-RAD (Bio-Rad Laboratories Ltd., Hemel Hempstead, UK) was used to determine the oligomeric state of the size exclusion fractions. The electrophoresis was carried out using a Mini PROTEAN^{R} Tetra Cell (Bio-Rad Laboratories Ltd., Hemel Hempstead, UK). To make the proteins visible the gel was stained for 10 min with a solution of 0.5% Commassie R brilliant blue, 50% ethanol and 10% acetic acid and then destained with hot water over night.

2.3.2.1. bMGL

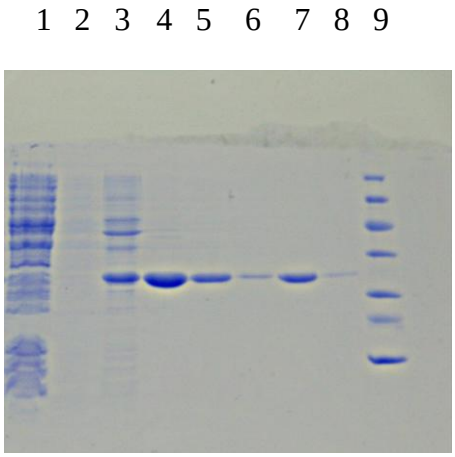

Figure 15 bMGL Ni-NTA purification. . 1=loading flow through, 2= first drop of washing fraction, 3= after 5 CV of washing, 4=last drop of washing fraction, 5=first drop of elution, 6= elution after 2.5 CV, 7= last drop of elution, 8= dialysate, 9= unstained protein marker

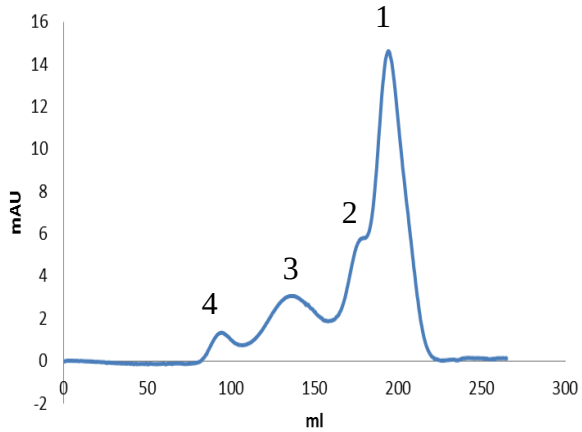

Figure 14 bMGL wild type size exclusion chromatography. 1= monomer, 2= dimer, 3= hexamer, 4=aggregate

After purification using a Ni-NTA raisin bMGL wt was isolated from any significant contaminations (Figure 15). The size exclusion chromatogram shows 4 different states of the protein. Only the monomeric fraction was used for further experiments.

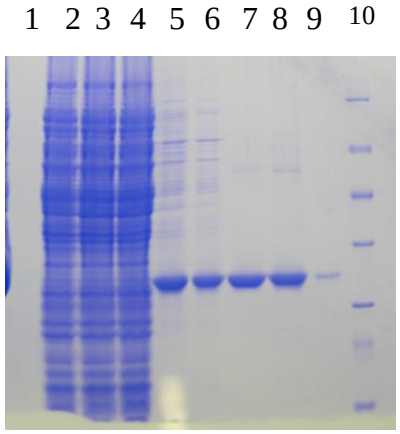

Figure 16 bMGL D196N Ni-NTA purification and SEC fractions. 1= first drop of loading, 2= half volume of loading, 3= last drop of loading, 4= first drop of washing, 5= washing after 5 CV, 6= last drop of washing, 7= first drop of elution, 8= elution after 2.5 CV, 9= last drop of elution, 10= unstained protein marker

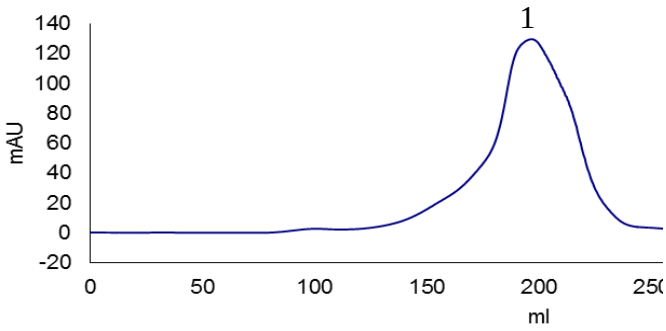

Figure 17 bMGL D196N size exclusion chromatography 1= monomer

The bMGL D196N mutant was purified to a very high degree (Figure 16) and fortunately

only showed one peak during size exclusion chromatography (Figure 17). This peak corresponds to the molecular weight of monomeric protein.

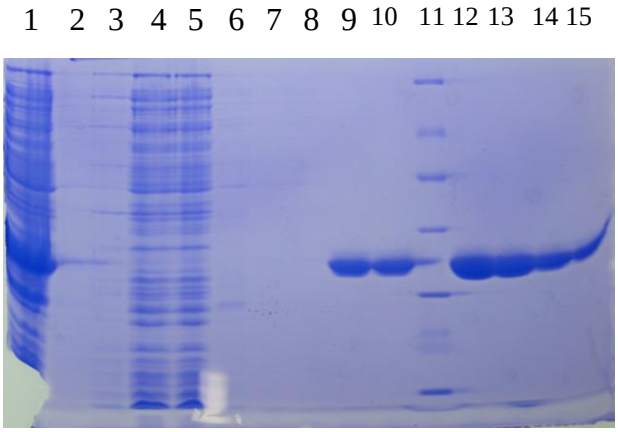

Figure 18 bMGL I145S Ni-NTA purification and SEC. purification 1= centrifuged filtered lysate, 2= first drop of loading, 3= middle of loading volume, 4= last drop of loading, 5= washing first drop, 6= washing after 5CV, 7= last drop of washing, 8= elution first drop, 9=elution after 2.5CV, 10=last drop of elution, 11= unstained protein marker, 12=fraction67, 13= fraction69, 14=fraction71, 15=fraction73

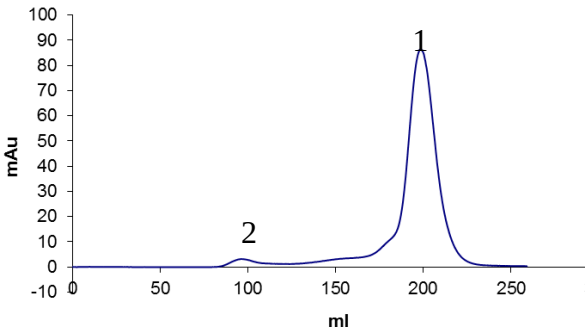

Figure 19 bMGL I145G size exclusion chromatography. 1= monomer, 2=aggregate

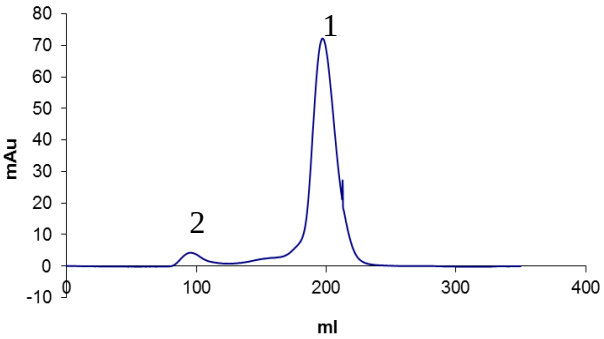

Figure 20 bMGL I145S size exclusion chromatography. 1= monomer, 2= aggregate

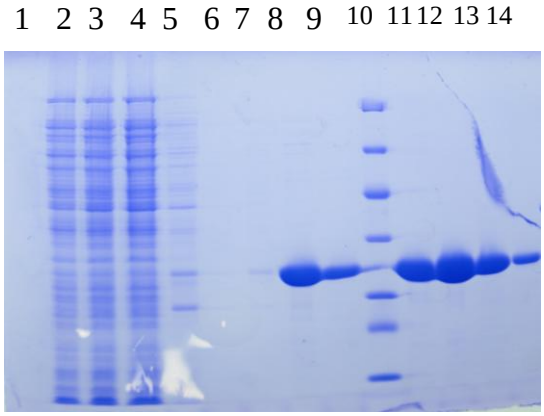

Figure 21 bMGL I145G Ni-NTA and SEC fractions.. 1= first drop of loading, 2= middle of loading volume, 3= last drop of loading, 4= washing first drop, 5=washing after 5CV, 6= last drop of washing, 7= elution first drop, 8=elution after 2.5CV, 9=last drop of elution, 10= unstained protein marker, 11= fraction62, 12= fraction66, 13= fraction70, 14= fraction74

The bMGL I145S mutant as well as the bMGL I145G mutant were isolated of any protein contaminations (Figure 18, Figure 21). The size exclusion chromatography revealed a monomeric and an aggregate peak. The monomer was used for further experiments.

2.3.2.2. YJU3L171S

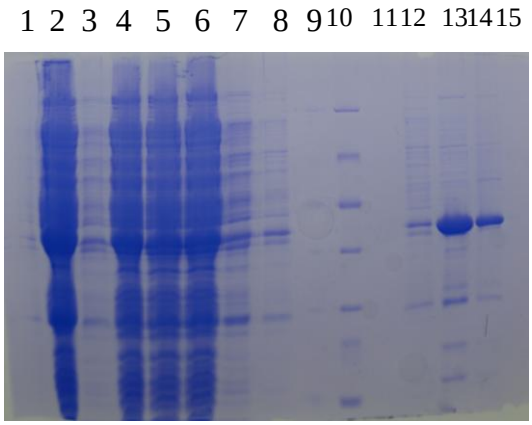

Figure 22 YJU3L171S Ni-NTA purification. 1= empty, 2= lysate, 3= first drop of loading, 4= middle of loading volume, 5= last drop of loading, 6= first drop washing, 7= washing after 5CV, 8=last drop washing, 9=empty, 10= unstained protein marker, 11= empty, 12= first drop elution, 13= elution after 2.5CV, 14= last drop elution, 15= empty

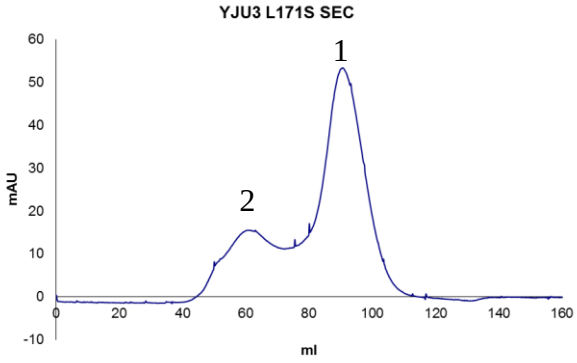

Figure 23 YJU3 L171S size exclusion chromatography. 1= monomer, 2= aggregate

Figure 22 shows that Ni purification of YJU3 L171S did not work as good as for the other protein. The elution (lanes 12-14) showed clearly more than one band. The size exclusion chromatogram showed some aggregate, but most of the protein was in a monomeric state.

2.3.2. Crystallization, data collection and refinement

2.3.2.1. bMGL wt

Since bMGL shows higher activity for substrates with longer carbon chains the first choice for co-crystallization experiments was C_{12}. Dataset quality crystals (Figure 24) were obtained in the same condition the free form of bMGL wt was crystallised (31).

Figure 24 Crystals of the bMGL C12 complex.

Unfortunately the co-crystallisation of bMGL with substrate analogues with longer carbon chains in the condition mentioned above turned out to be more difficult; thus the search for a new crystallisation condition began. The first crystallisation experiments were done with free bMGL. The initial crystal obtained from a JCSG+ screen (Figure 25) was unusable for X-ray diffraction measurements because it showed an overlap of hundreds of very weak diffraction patterns. In order to optimize this crystal the pH and the concentration of precipitant was varied. The resulting crystals (Figure 26) did not show any diffraction (probably because they were too small) but seemed to be solid rods instead of a fibre bundle (Figure 25).

Figure 25 Initial bMGL crystal in the JCSG+ condition A2

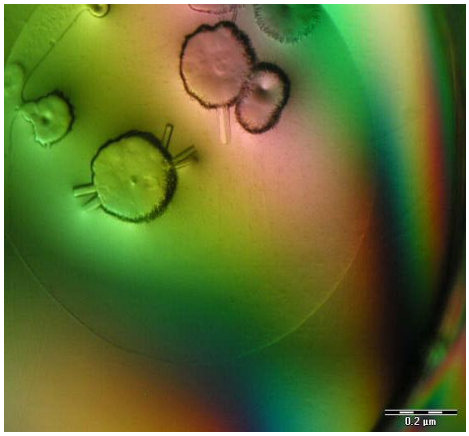

Figure 26 optimization of the initial JCSG+ A2 crystall

Since the original idea was to co-crystallise bMGL with substrate analogues, the next step was to co-crystallise C_{14} with bMGL in the new condition obtained so far (Figure 27). These

crystals were still too small and many of them were stuck to the bottom of the crystallisation plate; therefore they were optimized using the hanging drop method. The resulting crystals (Figure 28) diffracted to 1.85Å and were successfully used for data collection.

Figure 27 Optimized JCSG+ A2 crystals complexed with the C14 ligand

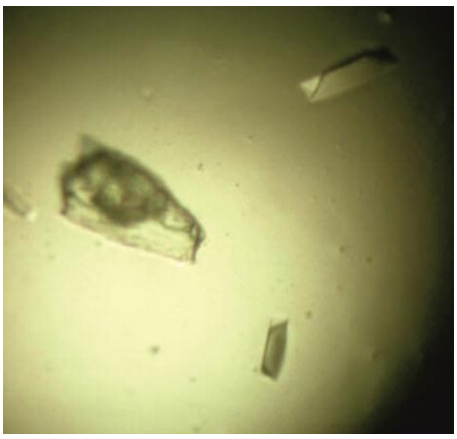

Figure 28 Hanging drop optimization of the JCSG+ A2 crystals with C14

Contents	**bMGL-C_{12} complex**	**bMGL-C_{14} complex**
Data collection		
Wavelength (Å)	0.81	1.0
Resolution (Å)	25.0 – 1.7	43.7 – 1.85
Space group	$P2_1$	$P2_1$
Unit-cell parameters a, b, c (Å) β (°)	 43.8, 71.2, 72.9 102.0	 77.0, 81.1, 85.6 100.3
Total number of reflections	143465	293651
Unique reflections	47227	88070
R_{sym}	0.065	0.057 (0.30)

Completeness (%)	96.9 (87.8)	99.5 (99.6)
Mean I/σ(I)	8.7 (4.2)	17.9 (4.2)
Multiplicity	3.0 (2.8.)	3.4 (3.3)
Refinement statistics		
No. of protein atoms	3853	7668
No. of solvent molecules	439	1200
R_{cryst}	18.5	21.9
R_{free}	22.0	24.2
Model geometry		
RMSD bonds (Å)	0.011	0.013
RMSD angles (°)	1.309	1.378
Ramachandran distribution		
Most favoured (%)	97.3	97.5
Additionally allowed (%)	2.7	2.5
Outliers (%)	0.0	0.0

Table 6: Crystal parameters and data collection statistics are derived from SCALA (Evans, 2006). To calculate R_{free}, 5% of the reflections were excluded from the refinement. R_{sym} is defined as $R_{sym}=\Sigma_{hkl}\Sigma_i|Ii(hkl)-\langle I(hkl)\rangle|/\Sigma_{hkl}\Sigma_i Ii(hkl)$. Data in parentheses correspond to the highest resolution shells

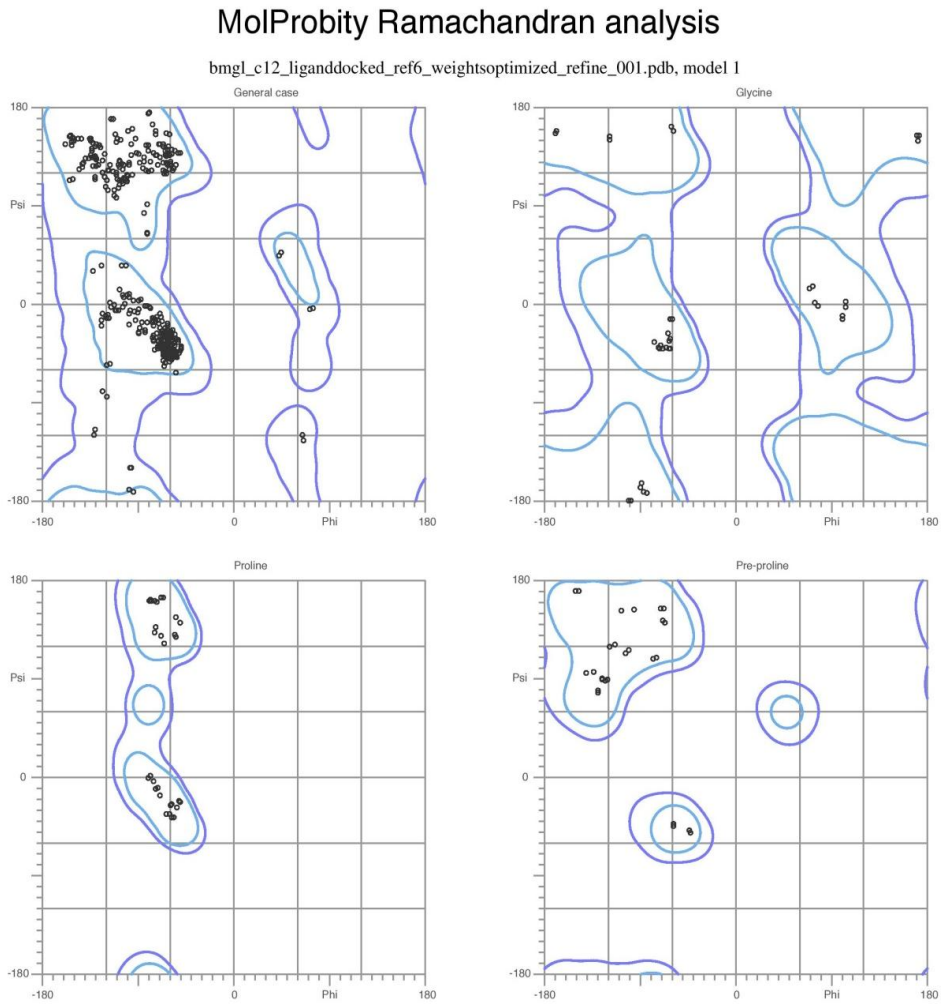

97.8% (482/493) of all residues were in favored (98%) regions.
100.0% (493/493) of all residues were in allowed (>99.8%) regions.

There were no outliers.

Figure 29 Ramachandran plot bMGL-C12 complex

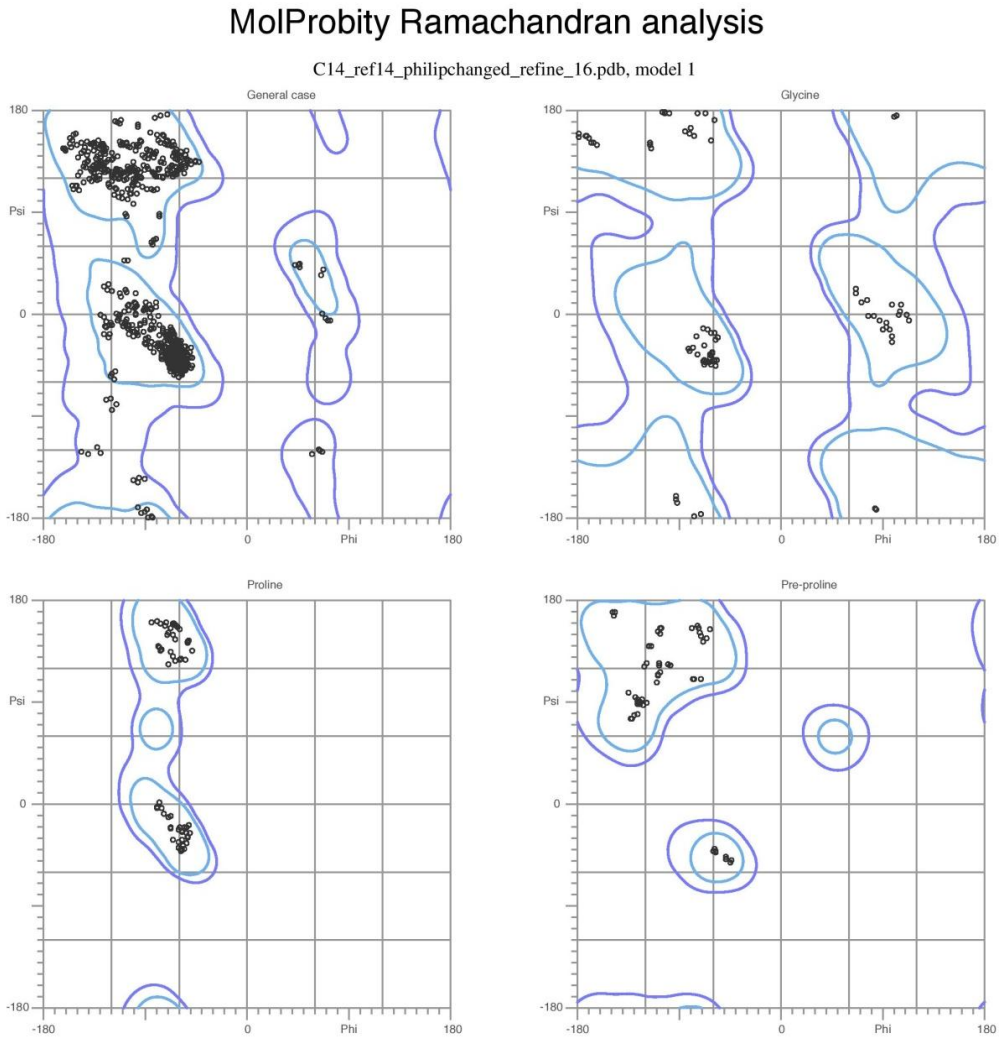

97.8% (963/985) of all residues were in favored (98%) regions.
100.0% (985/985) of all residues were in allowed (>99.8%) regions.

There were no outliers.

Figure 30 Ramachandran plot bMGL-C14 complex

The free form of bMGL also gave beautiful crystals in this new crystallisation condition (Figure 31). Unfortunately the resolution of the resulting data set (2.5Å) was significantly lower than for the bMGL-C_{14} complex.

Figure 31 bMGL free form crystals in optimized JCSG+ A2 condition

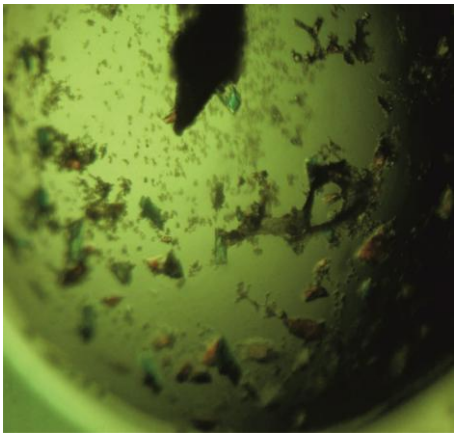

Figure 32 Crystal of bMGL in complex with C16

In order to cocrystallise bMGL with C_{16} this new crystallisation condition needed small modifications. After slight changes of the pH and the precipitant concentration crystalls diffracting to 2.2Å were obtained (Figure 32).

Contents	**bMGL-C_{16} complex**	**Free bMGL in C_{14} condition**
Data collection		
Wavelength (Å)	0.98	0.81
Resolution (Å)	43.7-2.2	49.2-2.5
Space group	$P2_1$	$P2_1$
Unit-cell parameters a, b, c (Å) β (°)	 76.9 80.3 85.7 100.02	 77.3 81.5 85.7 100.5

Total number of reflections	339325	83234
Unique reflections	48702	34067
R_{sym}	0.14 (0.56)	0.105 (0.19)
Completeness (%)	93.2 (68.4)	93.9 (79.63)
Mean I/σ(I)	9.0(4.3)	6.5 (4.9)
Multiplicity	7.0 (4.8)	2.4 (2.8)
Refinement statistics		
No. of protein atoms	7384	7429
No. of solvent molecules	227	246
R_{cryst}	21.8%	25.1%
R_{free}	25.8%	30.6%
Model geometry		
RMSD bonds (Å)	0.004	0.026
RMSD angles (°)	0.952	2.257
Ramachandran distribution		
Most favoured (%)	96.4	91.5
Additionally allowed (%)	3.6	7.4
Outliers (%)	0.0	1.1

Table 7: Crystal parameters and data collection statistics are derived from SCALA (Evans, 2006). To calculate Rfree, 5% of the reflections were excluded from the refinement. Rsym is defined as Rsym=ΣhklΣi|Ii(hkl)−⟨I(hkl)⟩|/ΣhklΣiIi(hkl). Data in parentheses correspond to the highest resolution shells.

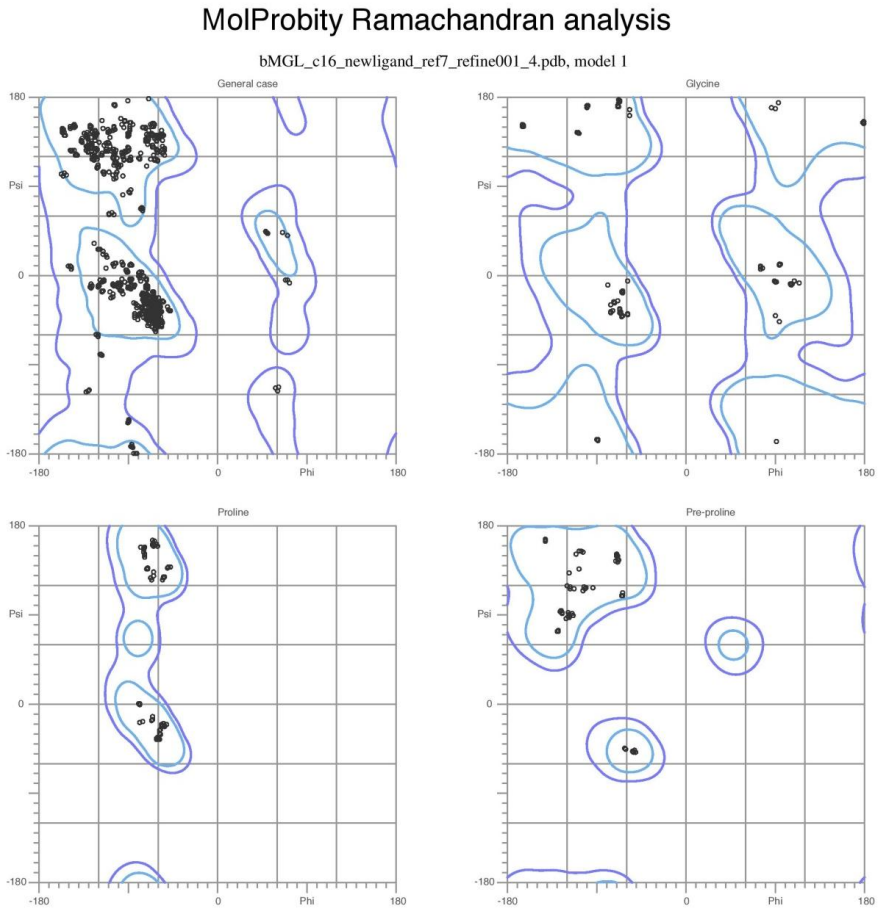

96.4% (940/975) of all residues were in favored (98%) regions.
100.0% (975/975) of all residues were in allowed (>99.8%) regions.

There were no outliers.

Figure 33 Ramachandran plot bMGL-C16 complex

2.3.2.2. bMGL D196N mutant

The initial crystals obtained for the bMGL D196N mutant in complex with 1-LG were needle clusters (Figure 34). Using a seeding stock made of these crystalls gave single crystalls in form of rods in the JCSG+ condition H12 (Figure 35).

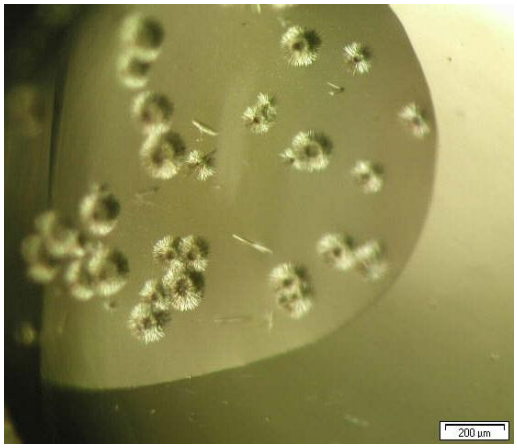

Figure 34 Initial crystals of the bMGLD196N mutant in Morpheus condition A4

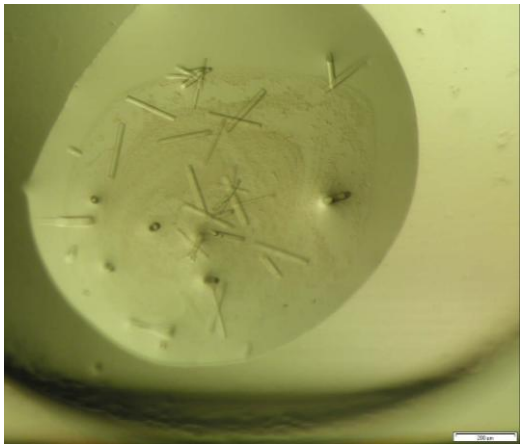

Figure 35 Crystal of the bMGL D196N mutant in JCSG+ H12 using microseeding.

Optimisation of these rods gave smaller but diffracting (8Å) crystals (Figure 36). To get bigger crystalls and therefore higher resolution this condition was improved using hanging drop setups. Finally dataset quality crystals diffracting to 1.85Å were obtained (Figure 37).

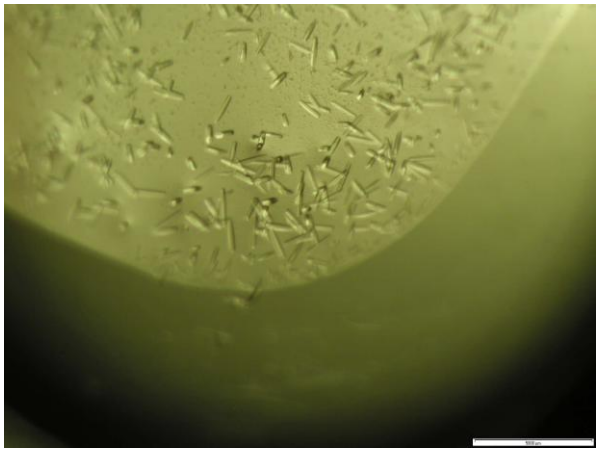

Figure 36 Sitting drop optimization of the bMGLD196N crystals in JCSG+ H12 using microseeding

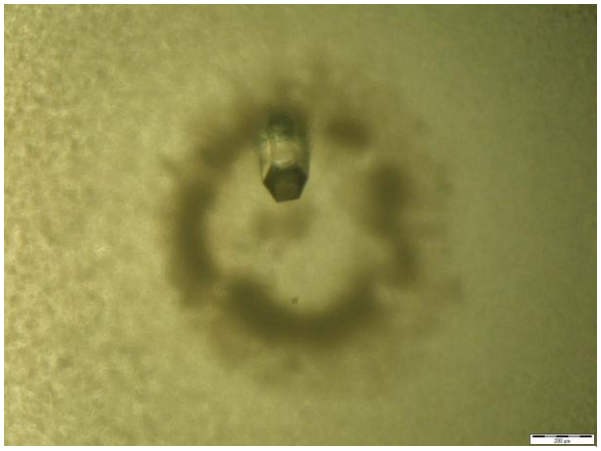

Figure 37 Final bMGLD196N crystal using hanging drop and microseeding.

Contents	**bMGLD196N 1-LG complex**
Data collection	
Wavelength (Å)	0.95
Resolution (Å)	43.7-1.85
Space group	$P3_1$ 2 1
Unit-cell parameters a, b, c (Å)	 191.2 191.2 77.3
Total number of reflections	1486823
Unique reflections	131923
R_{sym}	0.079 (0.405)
Completeness (%)	100 (100)
Mean I/σ(I)	13.3 (3.9)
Multiplicity	10.8 (7.2)
Refinement statistics	
No. of protein atoms	8503
No. of solvent molecules	717
R_{cryst}	15.7%
R_{free}	17.4%
Model geometry	
RMSD bonds (Å)	0.004
RMSD angles (°)	1.018
Ramachandran distribution	

Most favoured (%)	96.9
Additionally allowed (%)	3.0
Outliers (%)	0.1

Table 8 Crystal parameters and data collection statistics are derived from SCALA (Evans, 2006). To calculate Rfree, 5% of the reflections were excluded from the refinement. Rsym is defined as Rsym=ΣhklΣi|Ii(hkl)−⟨I(hkl)⟩|/ΣhklΣiIi(hkl). Data in parentheses correspond to the highest resolution shell

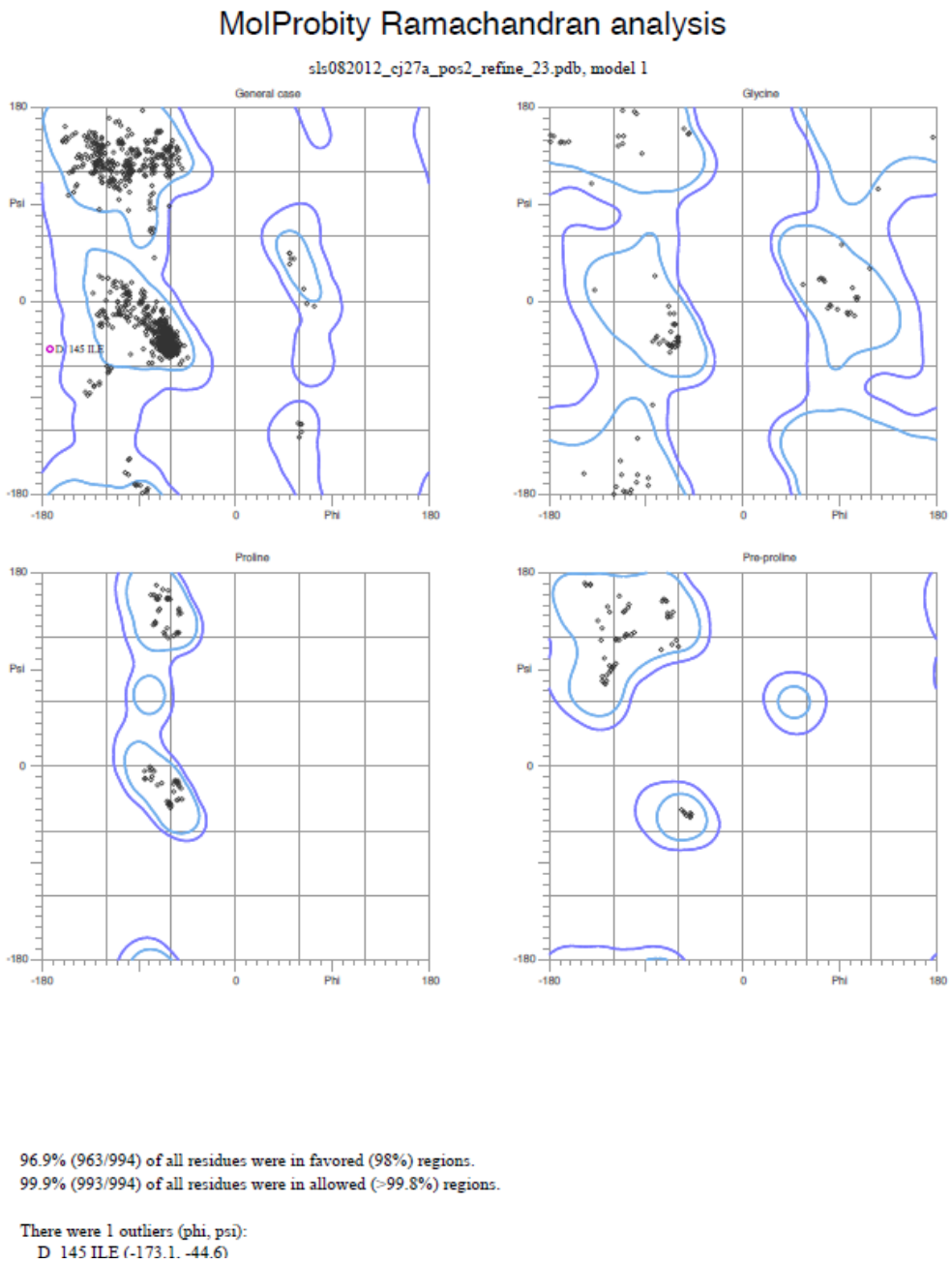

Figure 38 Ramachandran plot bMGLD196 1-LG complex

2.3.2.3. YJU3L171S mutant

The first YJU3 L171S crystal was the result of a crystallisation experiment set up by Christian Sturm. The crystal was a small cluster and showed no diffraction at all(Figure 39). Micro seeding using this crystal as seeding stock gave bigger crystals in the Morpheus condition C9 (Figure 40). This crystal was the first YJU3 L171S crystal to show protein diffraction (9Å).

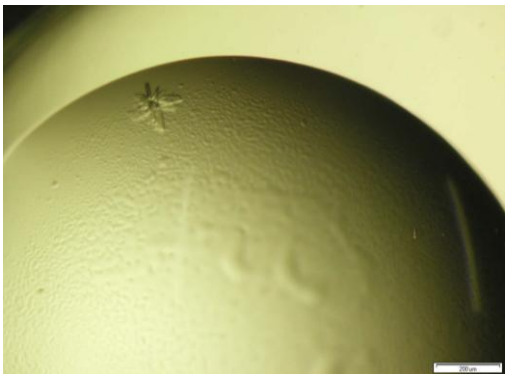

Figure 39 Initial crystal obtained in the Morpheus consition C5

Figure 40 Crystal in the Morpheus C9 condition with seeding

In order to get better resolution the pH of Morpheus condition C9 was optimized (Figure 42) followed by a hanging drop crystallization experiment(Figure 41). The final resolution was 2.7Å

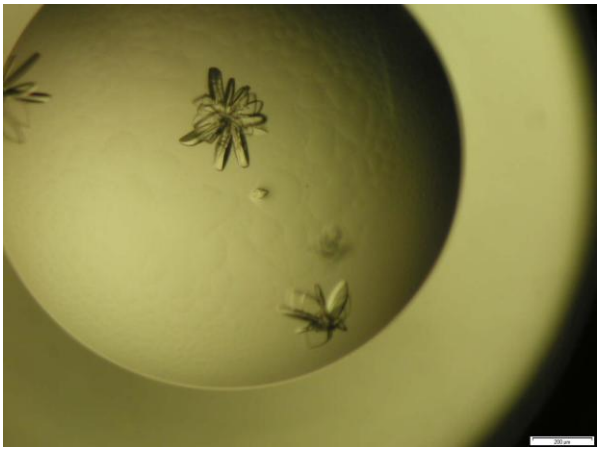

Figure 42 Optimized seeding condition for YJU3

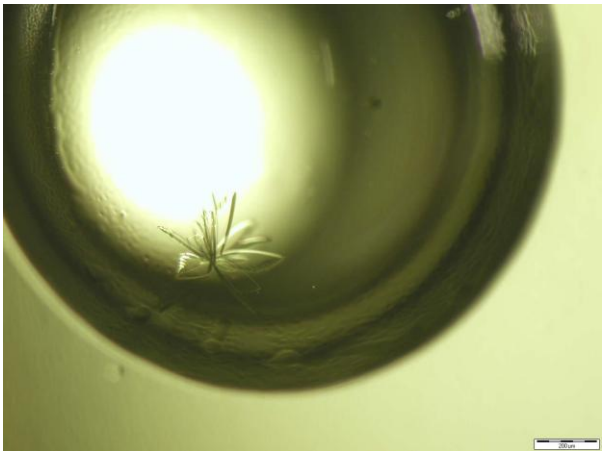

Figure 41 YJU3L171S in Morpheus C9 optimized with hangin drop.

Contents	**YJU3pL171S**
Wavelength (Å)	0.99
Resolution range (Å)	45.3-2.7
Unit cell parameters a, b, c (Å)	77.2, 108.6, 167.6
Space group	$P2_12_12_1$
Completeness	99.1 (99.0)
Multiplicity	8.1 (8.3)
R_{sym}	0.13 (0.65)
Mean[I/σ(I)]	12.7 (3.4)
Total number of reflections	317310
Total number of unique reflections	39013

Table 9: Crystal parameters and data collection statistics are derived from SCALA (Evans, 2006). To calculate Rfree, 5% of the reflections were excluded from the refinement. Rsym is defined as Rsym=ΣhklΣi|Ii(hkl)−⟨I(hkl)⟩|/ΣhklΣiIi(hkl). Data in parentheses correspond to the highest resolution shells.

2.3.3. 3D Structures of MGLs and their complexes

2.3.3.1. bMGL-C_{12} complex

The structures of an open conformation of bMGL in its free form and in complex with PMSF had already been determined in our group (31). Molecular Dynamics (MD) simulation showed that the cap of bMGL is quite flexible and therefore a closed conformation might be possible. The first idea behind a conformational change was substrate binding. Another reason that raised interest in substrate binding was to find out how MGL form *Bacillus sp. H257* maintains different specificities towards substrates with different chain length. A structure of bMGL in complex with the inhibitor with a C_{12} carbon chain lengths was determined at a resolution of 1.7Å was obtained.

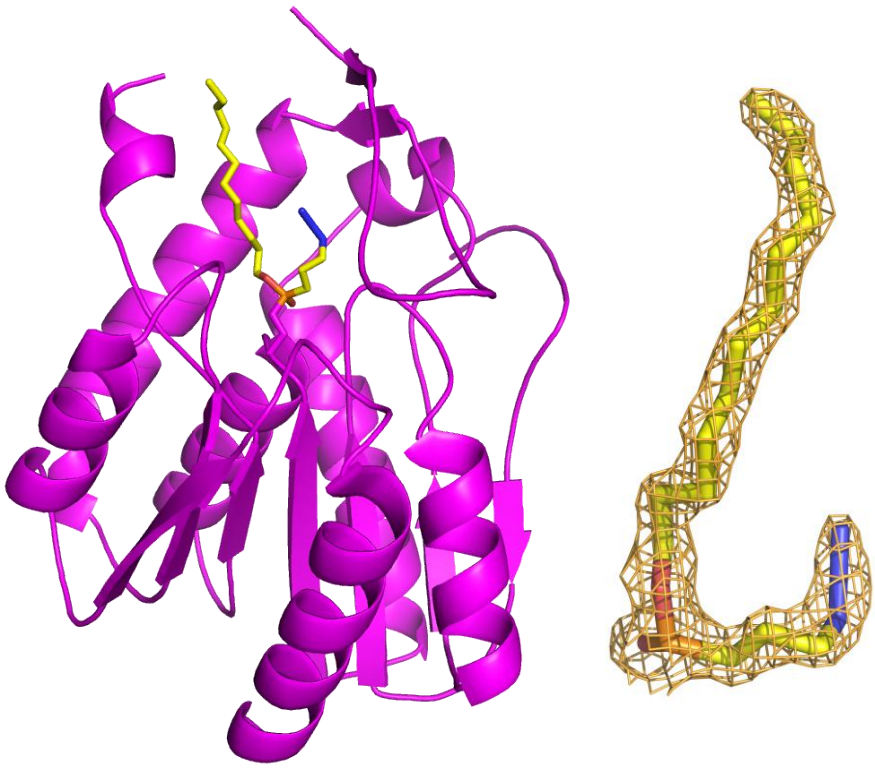

Figure 43 left) structure of bMGL (magenta) with C_{12} (yellow) covalently bound right) The 2Fo-Fc map of C_{12} ligand covalently bound to bMGL (chainA) contoured at 1σ (chain B)

The asymmetric unit of the bMGL-C_{12} complex structure was composed of two molecules; each of them showed clear electron density for the covalently bound C_{12} substrate analogue (Figure 43). It was not possible to observe the five missing residues (Thr133, Gly134, Gly135, Gly136, Asp137) in the cap region (31).The cap region was found to be in open conformation as seen before in the free form, meaning that the binding of the C_{12} substrate analogue did not trigger any conformational change.

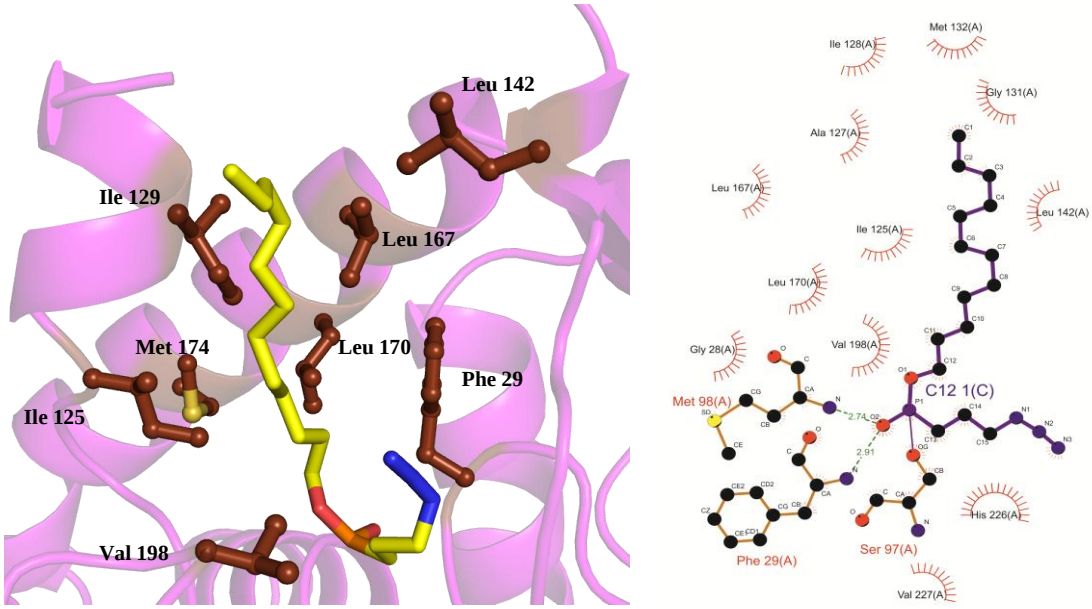

Figure 44 left.) Hydrophobic residues interacting with the C12-ligands carbon chain right) detailed look at the interactions in the binding pocket.

A more detailed look at the interactions of the ligand with residues of the binding pocket revealed the residues involved in hydrophobic interaction with the flexible carbon chain of the ligand, holding it in position and protecting it from contact with water (Figure 44(left)). Figure 44 (right) also provided a detailed view on the polar interactions with the head group, for example the stabilization of the phosphonate oxygen at the position of the oxyanion hole by the backbone nitrogen of Met98 and Phe29.

2.3.3.2. bMGL-C_{14} complex

The co-crystallization of bMGL with the C_{14} ligand took us one step closer to the understanding of the chain length specificity of bMGL. The C_{14}-complex crystals were obtained in a different crystallization condition with pH values of 5.2 (compared to pH 6.5 for

the C_{12}-complex condition) these differences, changes in ligand and changes in crystallization condition, could both result in conformational changes. The structure of the bMGL-C_{14} complex was solved at a resolution of 1.85 Å.

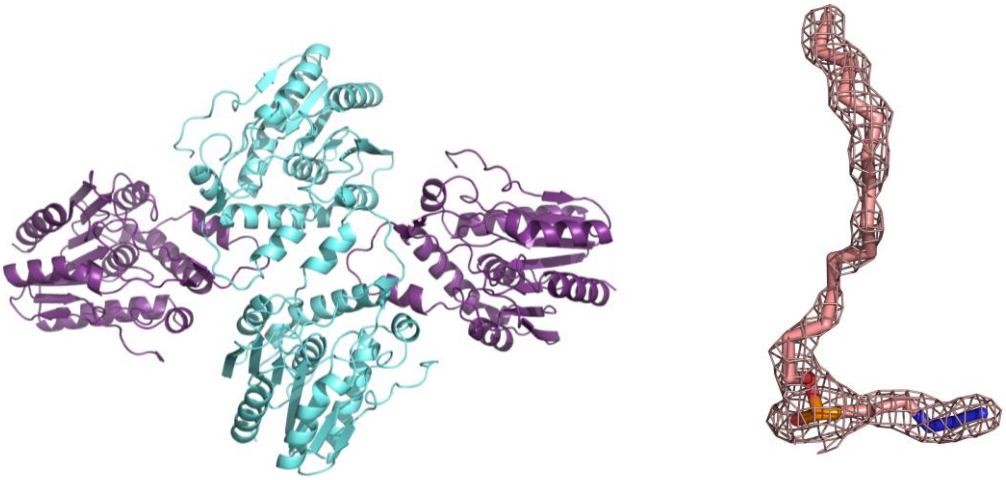

Figure 45 left) Structure of the bMGL-C_{14} complex, chain A and B in cyan, chain C and D in violet. right) 2Fo-Fo map of C_{14} ligand covalently bound to bMGL contoured at 1 σ (chainC).

This structure was the first structure in which electron density for all the residues in the cap region could be observed. The asymmetric unit was composed of 4 molecules, were each molecule showed electron density for the C_{14}-ligand (Figure 45). The packing showed two equal molecules twice (chain A and B, chain C and D). Interestingly chains A and B showed a slightly different conformation in the cap region than chains C and D. A closer look revealed, that both of these conformations are different to the one observed in the C_{12}-complex structure. The conformation in chains A and B will be called conformation II from now on, the conformation in chains C and D will be referred to as conformation III.

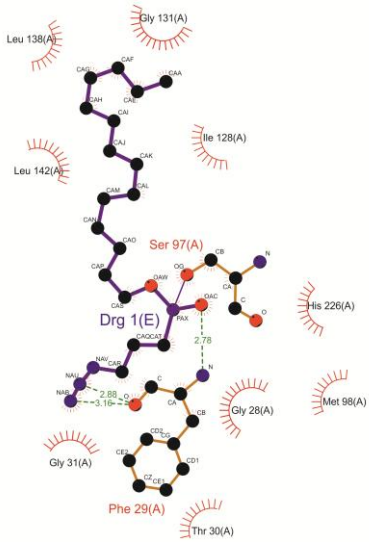

Figure 46 detailed look at the interactions in the substrate binding pocket.

The C_{14} complex revealed detailed information about the hydrophobic interactions between carbon chain and the hydrophobic side chains(Figure 46). We were

also able to observe electron density for the 5 residues (Thr133, Gly134, Gly135, Gly136, Asp137) that were missing before.

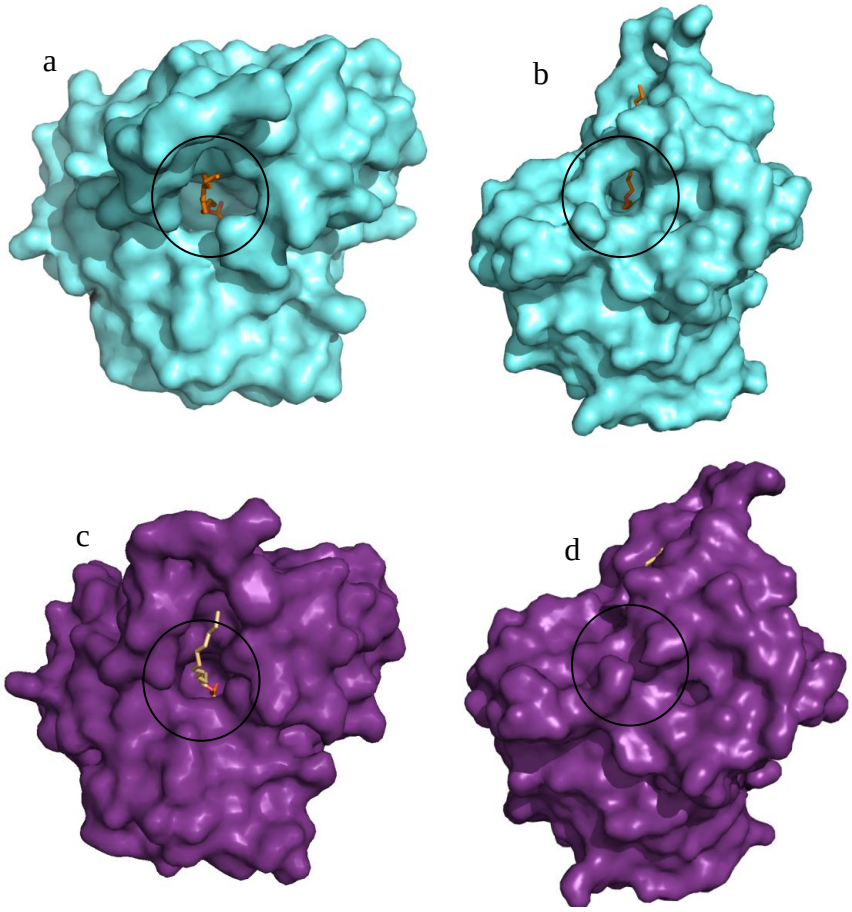

Figure 47 a) binding pocket chain A and B b) binding pocket chain C and D c) glycerol exit hole chain A and B d) glycerol exit hole chain C and D

One interesting thing about the bMGL-C_{14} complex was that it also revealed two new conformations for the cap region. Figure 47a). Figure 47a shows conformation II which shows a partially restricted conformation for the substrate binding pocket, b) points out, that conformation II showed an open glycerol exit hole. Conformation III showed a restricted conformation of the substrate binding pocket (Figure 47c). The constriction of the substrate binding pocket in conformation III also has an effect on the glycerol exit hole, which seems to close during this conformational change.

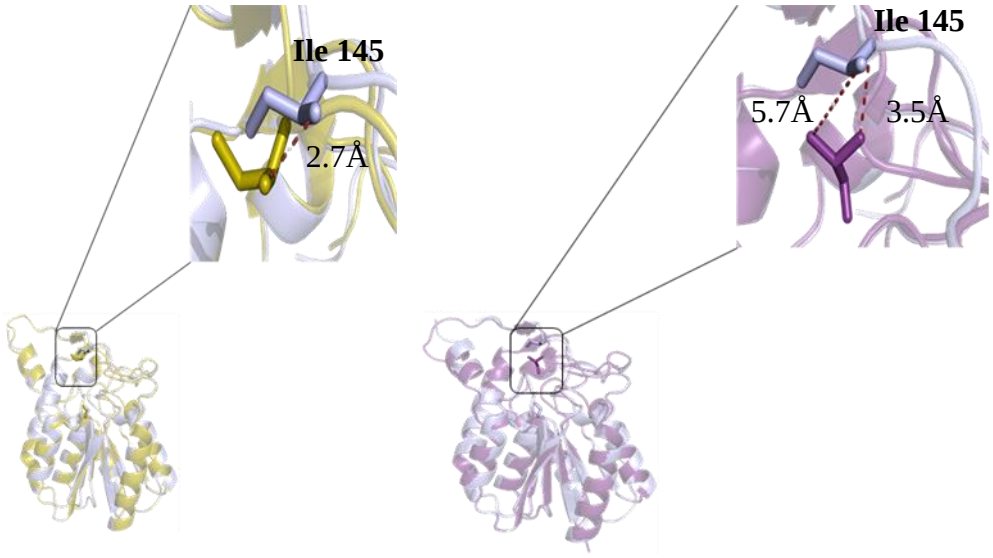

Figure 48 light blue) C_{12} structure, open conformation, yellow) C_{14} structure chain A and B, partially constricted, violet) C_{14} structure chain C and D, constricted conformation

A closer look at the areas involved in the conformation changes (Figure 47 black circles), showed Ile 145 as the major player in these conformational changes. The partially constricted conformation shows a rather small movement in the protein back bone with respect to the bMGL-C_{12} complex, while the restricted conformation was mediated by a big change in the backbone chain and a big flip of the Ile 145 side chain closing the glycerol exit hole.

In order to determine if the conformational change of Ile145 was caused by crystal packing or something else free bMGL was crystallised in the same condition as the bMGL-C_{14} complex. A resulting crystal was measured at ELETTRA (Trieste, Italy) to a resolution of 2.5Å. The structure showed the same conformation as the bMGL-C_{14} and bMGl-C_{16} structures.

This structure also raised an interesting question: the C_{14}-ligand (equal to a palmitoylglycerol in length) already locates close to the surface of the cap. Although bMGL has a lower specificity for longer chains it is still able to process oleoylglycerol. So the question is how do longer chains fit in the binding pocket? The answer is provided in the next chapter.

2.3.3.3. bMGL-C_{16} complex

We crystallised a bMGL-C_{16} complex, collected a data-set at ESRF (Grenoble, France), solved the phase problem by molecular replacement and finally obtained a structure with a resolution of 2.2Å.

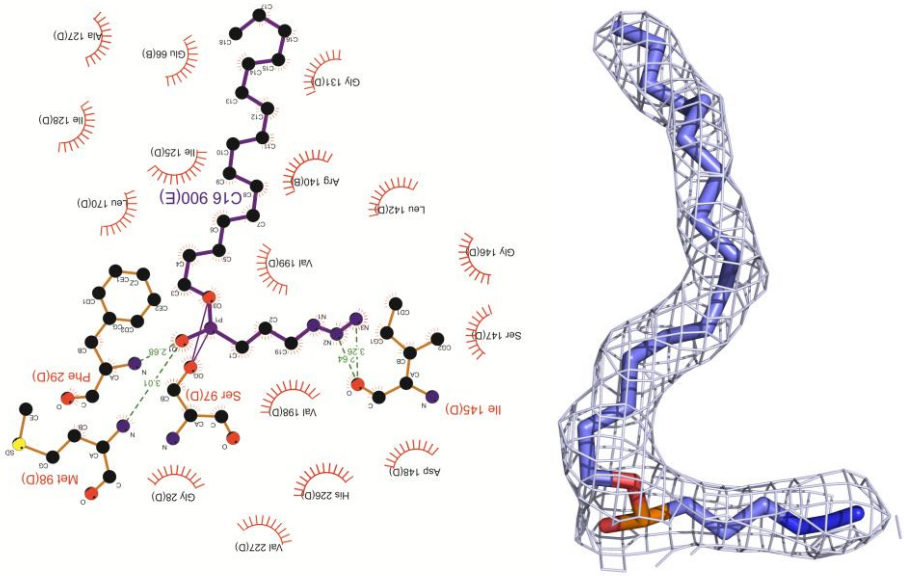

Figure 49 left) detailed view on the C_{16}-ligand binding in the binding pocket, right) 2Fo-Fc map of C_{14} ligand covalently bound to bMGL contoured at 1 σ (chain C).

The asymmetric unit of the bMGL-C_{16} complex was also composed of 4 molecules with the same conformations as in the bMGL-C_{14} complex. Figure 49 shows a detailed view of the interactions between ligand and protein in the binding pocket.

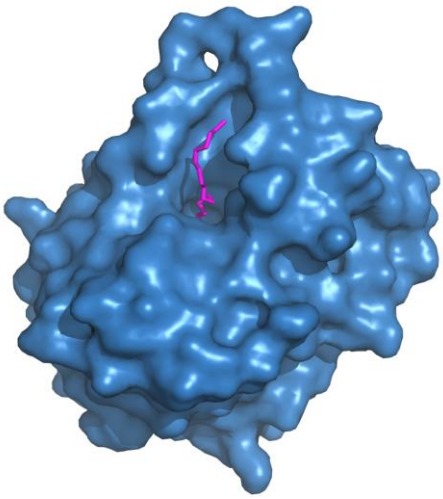

Figure 50 surface representation of bMGL-C_{16} complex

Interestingly the C_{16} chain, although it is longer than the C_{14} chain, seems to occupy the same space as the C_{14} chain.

2.3.3.5. bMGL D196N 1-LG complex

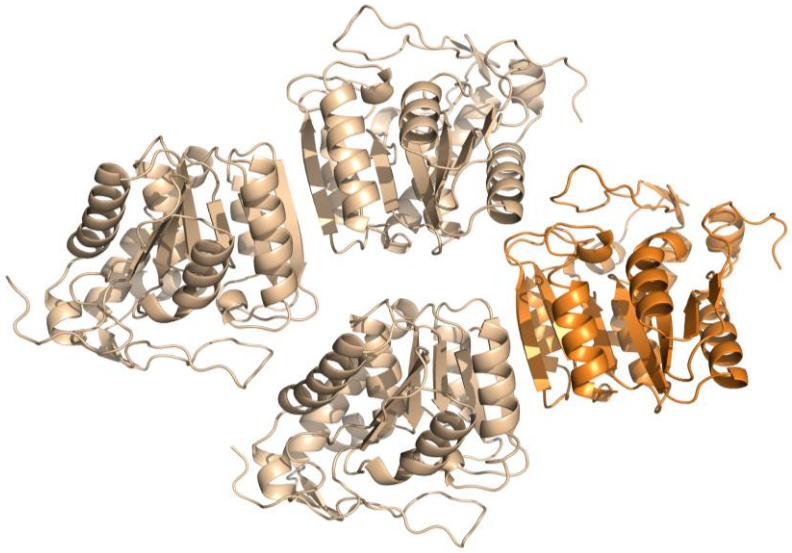

Figure 51 Asymmetric unit of bMGL D196N crystals, wheat= chain A, B, C; orange=chain D

After co-crystallisation of bMGL with the substrate analogues, a bMGL D196N mutant was created in order to stall the hydrolase activity and get the chance to trap the actual substrate inside the enzyme. The co-crystallization of this inactive bMGL D196N mutant with the actual substrate 1-lauroylglycerol was the most promising next step for a better understanding of the substrate binding, especially in respect to the interactions of the glycerol moiety. The final crystals diffracted to 1.85Å and the structure was solved by molecular replacement.

The asymmetric unit of the bMGL D196N structure was composed of 4 molecules (Figure 51). It seems that there are two dimers which were held together by packing the 7 β-strands of each molecule to a 14-fold β-strand. The interaction between the 2 dimers is facilitated by interactions of Arg222 and Asn223 in chain A (and D) with the backbone oxygen of Glu108 and the side chains of His110 and Glu78 in chain B (and C) (Figure 52).

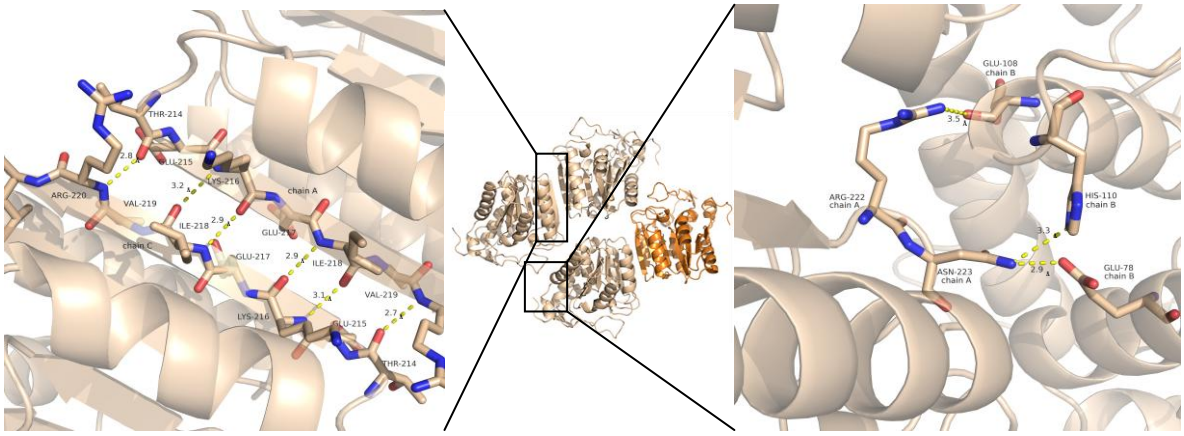

Figure 52 left) chainA – chainC interface; right) chainA – chainB interface

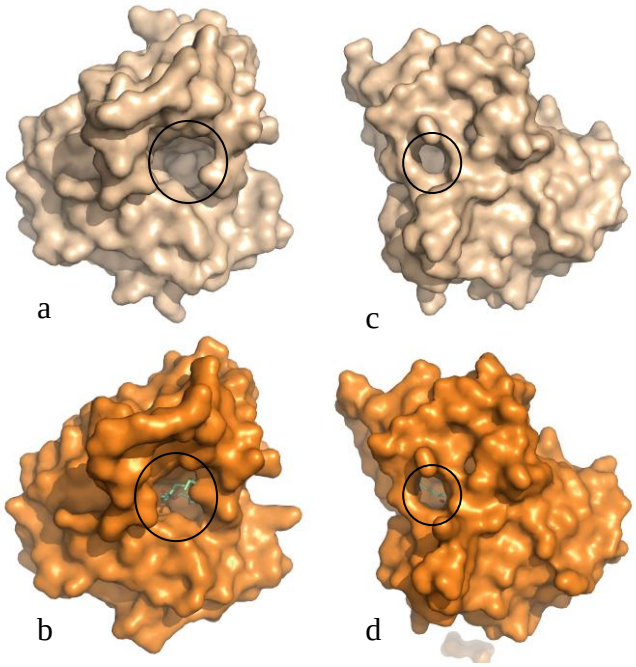

Figure 53 a) substrate binding pocket chains A,B,C b) substrate binding pocket chain D c) glycerol exit hole chains A,B,C d) glycerol exit hole chain D

The four chains of bMGL D196N showed two different conformations. The conformation found in the chains A, B and C is similar to the conformation observed in the bMGL-C_{12} complex (conformation I). Interestingly only chain D showed the same conformation as in chains A and B from the bMGL–C_{14} complex (conformation II) i.e. partial restriction of the substrate binding pocket around the substrate (A→D RMSD=0.141, B→D RMSD=0.159, C→D RMSD=0.158). The glycerol exit hole was open in all of the chains. The electron density around the loop region of the cap was poorly defined as a result of that electron density for the residues (Thr133, Gly134, Gly135, Gly136, Asp137) could not be observed.

This structure gave us the opportunity to have a look at a complex of an MGL with its actual substrate for the first time. Chain D was the only chain containing the substrate the other chains had MPD molecules from the crystallisation condition inside the substrate binding pocket. The electron density for the head group was well defined, information for the carbon

atoms 8 and 9 of the carbon chain was missing (Figure 54b, c). Hydrophobic interactions of the carbon chain with apolar residues in the substrate binding pocket stabilize the alkyl chain of 1 LG as observed for the substrate analogues. Additionally, the glycerol moiety of 1-LG seems to be stabilized by hydrogen bridges with hydrophilic amino acids at the bottom of the substrate binding channel (Figure 54a). The backbone nitrogen of Phe29 and Met98 are stabilizing the oxygen in the oxyanion hole like in the other bMGL structures. A close observation of the glycerol moiety identifies Glu156 as the side chain that holds the glycerol moiety in place.

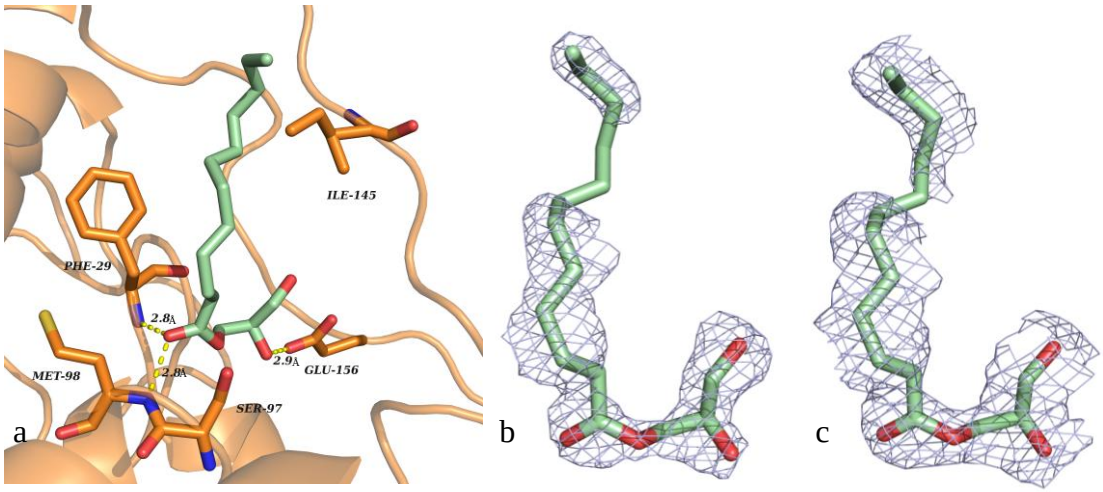

Figure 54 a) Interaction of 1-LG with the bMGL D196N substrate binding pocket b) 2Fo-Fc map of 1-LG contoured at 1 σ c) 2Fo-Fc map of 1-LG contoured at 0.5 σ

2.4. Discussion

2.4.1. Chain length specificity

One of the first questions to arise from bMGL was how the chain length specificity is maintained on a structural level. The biological explanation for specificity is quite clear since monoglycerides are toxic for bacteria, especially ones with shorter chains (27-30). Thus there is a marked higher specificity for short chain MGs. However the structural explanation for this chain length specificity was unclear till now. Since we were able to co-crystalize bMGL with substrate analogues with different chain length, we had the opportunity to perform a structural analysis of the behaviour of the substrate chains when bound to the enzyme. The

structure of the bMGL-C12 complex gave a first insight into the amino acid residues involved in stabilizing the carbon chain inside the substrate entrance channel. These hydrophobic interactions include Ile129, Leu142, Leu167, Leu170, Phe29, Met174, Ile125 and Val 198 (Figure 43). The crystal structure of the bMGL-C_{14} complex shows that the tail of a C_{14} carbon chain already localizes close to the surface of the cap region and seems to be accommodated within the binding pocket by introducing a slight bend into the carbon chain. Interestingly the C_{16} ligand still fits inside the protein although it is longer than C_{14}. The C_{16} ligand also seems to get by with approximately the same length as C_{14} does. This seems to be facilitated by introducing an even stronger bend in the hydrophobic chain. This bend directs the carbon chain away from its favourable conformation. The bend is less favourable and could explain the lower activity for substrates with longer carbon chains.

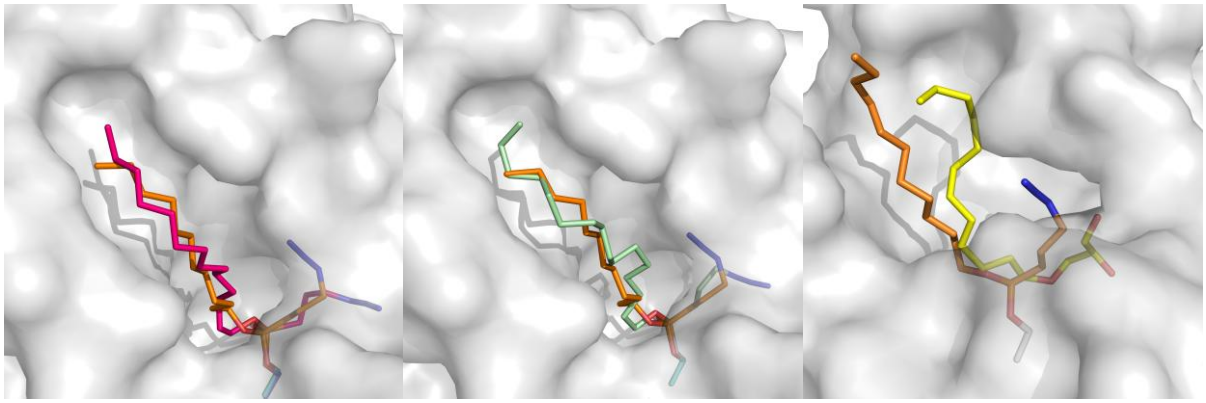

Figure 55 inhibitors bound to bMGL (grey surface), orange=C12, magenta=C14, light green=C16, yellow=1-LG

2.4.2. Conformational change

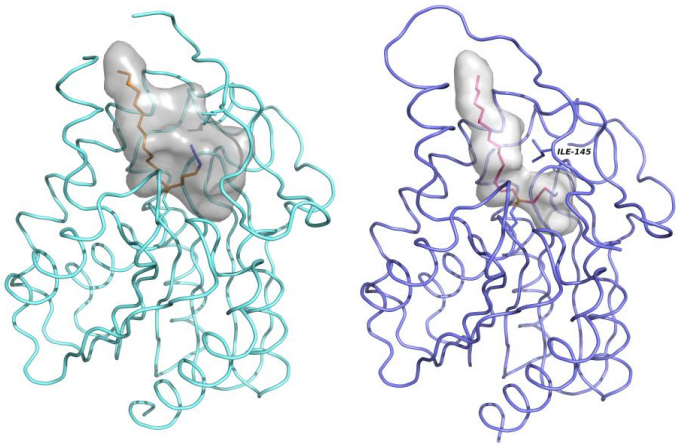

Figure 56 left) binding pocket open right) binding pocket restricted

Another characteristic of the C12 and the C14 complexes that needs to be pointed out is that the C14 complex was crystallised in a different condition. A closer look at the crystal structures (C14, C16 and free form in C14 condition) obtained from this condition exhibits changes in the conformation of the cap region (Figure 47). This change in conformation brings a restriction of the entire substrate binding pocket, making it impossible to fit anything else but the actual substrate.

A closer look at the conformational changes reveals that there are actually three conformations an open, a partially restricted, and a restricted one. Majority of the movement is mediated by a motion of the side chain of Ile145 and at a movement that is also accompanied by the backbone movement (Figure 48).The question arising from these observations are, what effects do this conformational change have, how is it facilitated and is there any preferential state of the enzyme in unbound state?

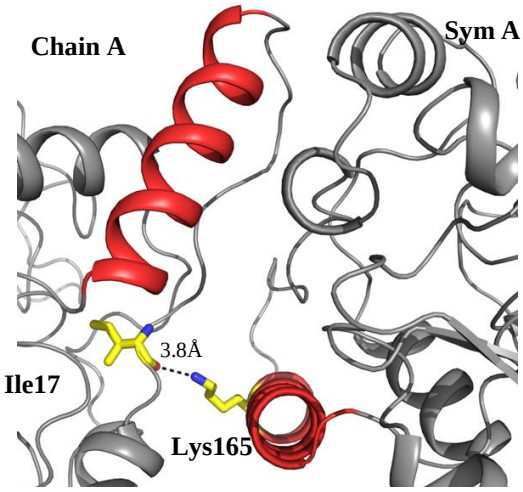

Figure 58 Crystal contacts in hMGL

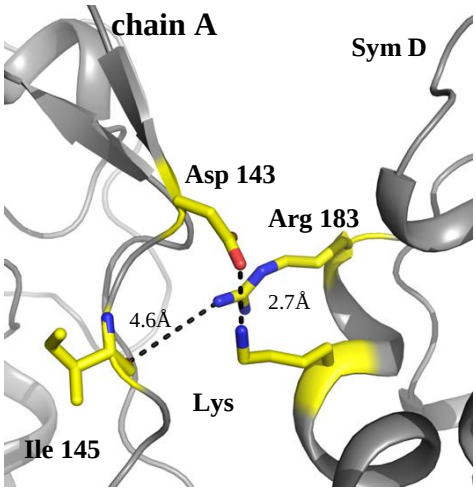

Figure 57 Crystal contacts in free bMGL in C14 condition

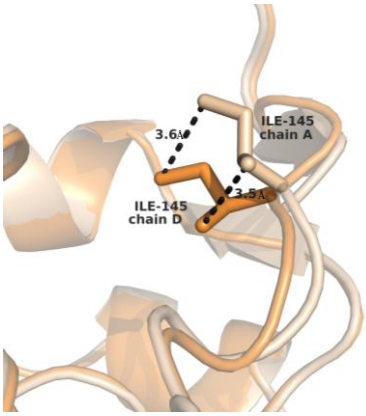

Figure 59 Conformational change in bMGL D196N. Orange = chain D, wheat = chain A

The first idea was that the conformational change is somehow influenced by the binding of the longer carbon chain of the C14 ligand. To test if this theory is valid free bMGL was crystallised in the same condition as the bMGL-C14 complex. This structure showed the exact same conformational changes, which proves, that the movement

of Ile 145 is not influenced by the ligand at all. Comparison with the closed conformation structure of hMGL (46) would suggest that the conformational change might be influenced by crystal packing. The closed conformation in the human structure seems to be stabilized by interaction of Ile179 backbone oxygen with the Lys165 side chain in the symmetry equivalent molecule (Figure 58). In bMGL on the other hand the residue of the crystal contact partner (symmetry equivalent chain D) nearest to Ile145 (equivalent to Ile179 in hMGL) is 4.6Å away which is too far for any interactions (Figure 57). Another argument why influence of the crystal packing on the conformational change is unlikely is the fact that the bMGL D196N 1-LG structure also shows the partially restricted conformation in one of the four chains. The reasons for the conformational change of Ile 145 in bMGL D196N 1-LG are still unclear. This is interesting because the crystals in C14 condition and the bMGL D196N crystal are not isomorph and crystallised in different space groups (P21 and $P3_221$ respectively). These results render crystal contacts an improbable reason Conformational changes in the cap region in bMGL D196N eliminate the possibility of an influence by the crystallization condition. For further investigation mutants of Ile145 were generated and will be investigated with respect to structure and enzymatic activity.

2.4.3. Glycerol stabilization

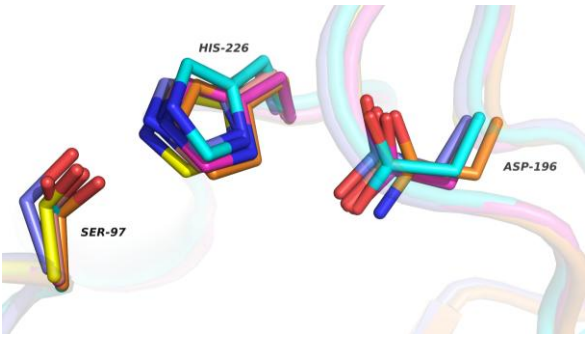

Figure 60 Overlay of the active site of all bMGL structures. Magenta= free bMGL structure by Srinivasan Rengachari (**31**), Cyan= free bMGL in C_{14} condition, Yellow= bMGL-C_{12} complex, Lightpink= bMGL-C_{14} condition, Blue= bMGL-C_{16} complex, Orange= bMGL D196N mutant 1-LG complex (Asn196 instead of Asp196)

In the covalently complexed structures we used substrate analogues to investigate the binding and orientation of the carbon chain. However, these analogues lack an actual glycerol moiety; so an obvious follow up question to investigate was: How would an actual substrate with glycerol in the head group behave inside the binding pocket? To answer this question Asp196 in the catalytic triad was mutated to an

Asn since it has the same size and shape, but handicaps catalytic reaction (because Ser97 cannot be deprotonated). Therefore this mutation should stall the substrate turnover without changing the arrangement of the catalytic site, as confirmed by our experimental structures (Figure 61). This way we were able to obtain a structure with a substrate molecule trapped inside the binding pocket. The substrate was only observed in one of the four chains in the asymmetric unit. This might be because the binding was not covalently like the analogue binding and therefor the substrate does not get trapped once it is inside the binding pocket. The complex structure of bMGL D196N in complex with 1-LG reveals that the carboxyl oxygen is stabilized in the oxyanions hole by the backbone nitrogen of Phe29 and Met98 as expected. The glycerol moiety seems to be held in place by a hydrogen bond between the hydroxyl group at position 2 and one of the side chain oxygens of Glu156. Mutations of Glu156 are carried out right now to further investigate the effect on substrate specificity and the enzyme activity. Additionally two conserved waters where found in 4 of the structures presented in this thesis (Figure 61). These two water form hydrogen bonds to the glycerol moiety of the bound substrate. Electron density for two of the carbons in the hydrophobic chain was missing, the reason for that might be that the substrate is not anchored to Ser97 any more like in the structures with the substrate analogues. This could result in increased mobility for the substrate and not clearly defined positions for these carbon atoms.

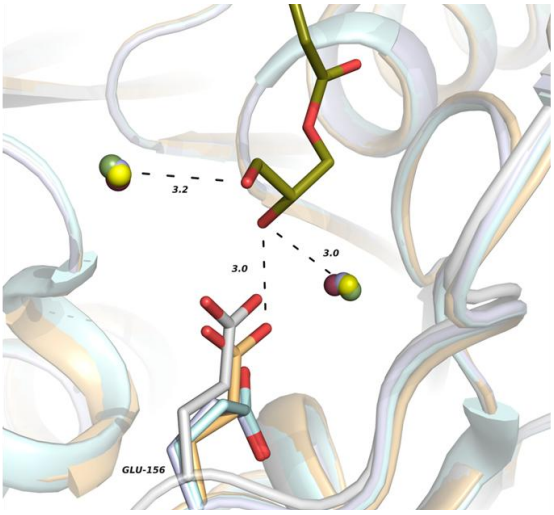

Figure 61 Overlay of freebMGL, C12 complex, C14 complex and 1-LG complex

3. Project HctB

This project was carried out in collaboration with Sarah Pratter and Grit Straganz from the Institue of Biotechnology and Biochemical Engineering at the University of Technology in Graz.

3.1 Introduction

HctB is one of the proteins encoded by the hct gene cluster in *Lyngbya majuscula*. The proteins of the hct gene cluster are involved in hectochlorine synthesis. HctB consists of an N- and a C-terminal domain and shows weak homology to phytanoyl Co-A hydroxylases a class of Fe^{2+}/2-oxoglutarate dependent hydrolases, and possesses all the amino acids necessary for the cofactor binding. The C-terminal domain is 35% identical to JamC, an acyl carrier protein in the jamaicamide gene cluster. HctB is suspected to form the gem-dichloro group in hectochlorin and therefore to be a halogenase (38).

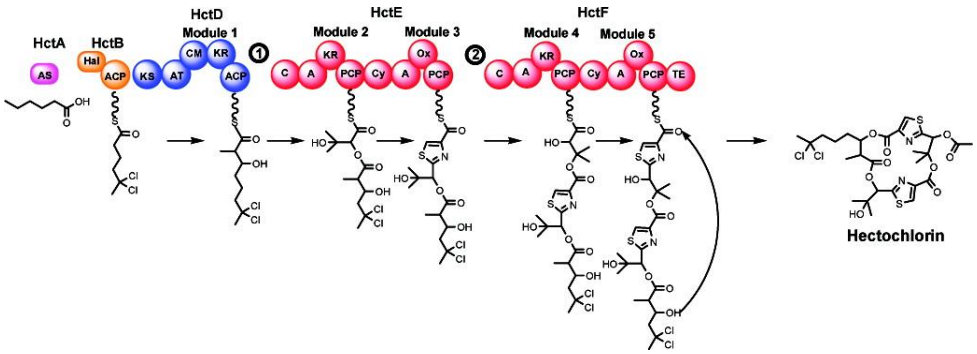

Figure 62 proposed schematic for hectochlorin synthesis in Lyngbya majuscule (38)

3.2. Methods

3.2.1. Protein Expression

<u>Media preparation</u>

Four solutions were prepared and autoclaved separately.

<u>Solution A:</u> 1.06g NH_4Cl + 25.75g $(NH_4)_2HPO_4$ + 23.20g KH_2PO_4 + 12.82g Na_2HPO_4 filled with Milli Q water to 1.8L.

<u>Solution B:</u> 50,05g glucose filled with MilliQ to 750ml.

Solution C: 50g yeast extract filled with MilliQ to 1950ml.

Solution D: 6.48g Ammonium Fe(II) citrate + 5.25ml SL6 trace element mix filled with MilliQ to 525ml.

Three overnight cultures were prepared containing 28ml solution A, 12ml solution B, 32ml solution C, 8ml solution D, 100µl Kanamycin (40mg/ml) and 330µl glycerol stock (received from Sarah Pratter, Institute for Biotechnology and Biochemical engineering, University of Technology, Graz, Austria) (HctB gene in IBA-pASK7plus vector, *E.coli* BL21DE3 gold cells). One additional flask with the same composition but without glycerol stock was used as negative control. These cultures were incubated at 37°C and shaken at 120rpm overnight.

The main culture consisted of 12 flasks containing 105ml solution A, 45ml solution B 120ml solution C, 30ml solution D, 375µL Kanamycin (40mg/ml) and 13.3ml overnight culture.

These solutions were incubated at 37°C and shaken at 120rpm until they reached an optical density (600nm) of 0.7. After cooling the cultures down to room temperature they were induced with 125µL 1M IPTG and incubated at 18°C and 120rpm for 20h.

The cells were harvested by spinning the suspension down with 4424g for 25min (Avanti J-26XP centrifuge, rotor JA 10, Beckman-Coulter GmbH, 47807 Krefeld, Germany). The pellet was resuspended in 36ml lysis buffer (50mM Tris pH8.5, 150mM NaCl, 5%Glycerol, 100mM Na_2CO_3) separated into 6 aliquots and stored at -20°C.

3.2.2. Purification

After a HctB cell aliquot (described in chapter 3.2.1. Protein Expression) was thawed it was homogenized using a (ULTRA TURRAX T25, IKA®-(Werke GmbH & CO. KG, 79219 Staufen, Germany) and sonicated (SONOPLUS HD 2070, BANDELIN electronic GmbH & Co. KG, 12207 Berlin, Germany) for 10 min with the settings Cycles=5 and Power=50%.The lysate was centrifuged (Avanti J-26XP centrifuge, rotor JA 25.50, Beckman-Coulter GmbH, 47807 Krefeld, Germany) for 45 min with 39191g at 4°C. The resulting supernatant was filtered through a 0.2µL syringe filter and the applied on a 1ml strep-tactin superflow column (QIAGEN GmbH, 40724 Hilden, Germany). The column was washed with 15 column volumes of NP buffer (50mM Tris pH 8.0, 300mM NaCl, 1mM TCEP) and eluted with 10

column volumes of NPD buffer (50mM Tris pH 8.0, 300mM NaCl, 1mM TCEP, 2.5mM d-desthiobiotin).

The flow-through resulting from the loading of the column was collected and re-issued onto the column three times.

The elution fractions were united, concentrated to approximately 10ml and applied on 250ml Superdex 200 resin (Pharmacia XK 26, GE Healthcare, Solingen, Germany) for size exclusion chromatography using a flow rate of 2ml/min, 2ml fractions were collected between ml 80 and ml 240 (size exclusion buffer: 50mM Tris pH 8,0; 300mM NaCl; 1mM TCEP).

The monomeric fractions were pooled, concentrated to approximately 15mg/ml stored at 4°C and used as soon as possible.

3.2.3. Crystallization

Complexing

0.26mM HctB was mixed with 30mM α-keto-glutaric acid to achieve a final protein/ αKG ratio of 1/2.5. This mixture was incubated for 10min on room temperature and then used for crystallization.

Crystallization

Initial crystals were obtained after 2 days from a Morpheus screen (Molecular Dimensions, Suffolk, UK) mixing 0.5µl HctB αKG mix with 0.5µl condition. The condition for this crystals was Morpheus H10 containing 10% w/v PEG8000, 20% v/v ethylene glycol, 0.1M amino acid mix and 0.1M Bicine/Trizma pH 8,5 **(**Figure 66Figure 65**)**. These crystals were very thin plates and therefore didn´t diffract; but they didn´t show any salt diffraction either, so they were considered to be protein. Also Izit dye (HR4-710, Hampton research, California, USA) stained them blue which is also an indication that they were protein crystals (Figure 65).

These crystals were used to create a seeding stock by mixing the drop with 50µl Morpheus H10 original condition and crushing them with a seed bead (HR2-320, Hampton research, California, USA).

Again a Morpheus screen was set up this time mixing 0.4µl HctB αKG mixture with 0.4µl condition and 0.2µl seeding stock 1:100 diluted. This setup gave thicker but clustered crystals after 2 days in condition H6 containing 10% w/v PEG8000, 20% v/v ethylene glycol, 0.1M amino acid mix and 0.1M MOPS/HEPES pH 7.5 (Figure 67).

3.3. Results

3.3.1. Purification

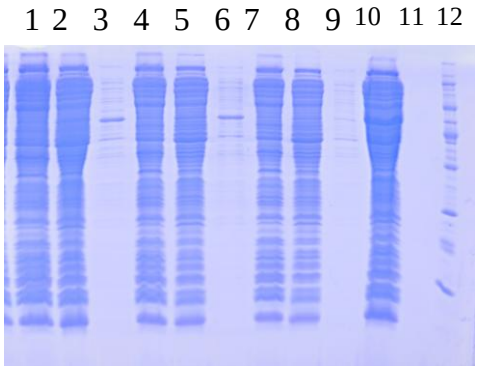

Figure 64 HctB Strep-tactin purification. 1=loading first cycle, 2= washing first cycle, 3= elution first cycle, 4= loading second cycle, 5= washing second cycle, 6= elution second cycle, 7= loading cycle three, 8= washing cycle three, 9= elution cycle three, 10= lysate, 11=empty, 12=unstained protein marker

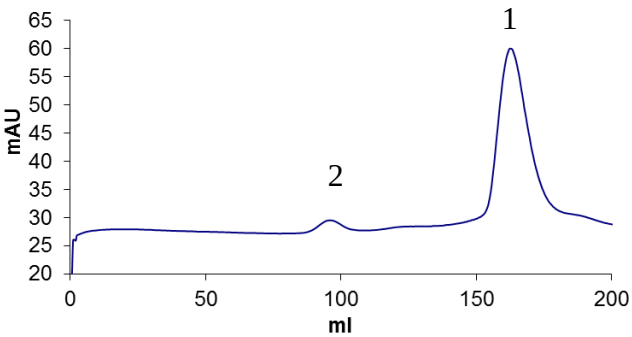

Figure 63 HctB size exclusion chromatogram. 1= monomer, 2= aggregate

It was possible to separate HctB from significant protein contaminations (Figure 64). The monomeric fraction was used for crystallization experiments (Figure 63peak 1).

3.3.2. Crystallisation

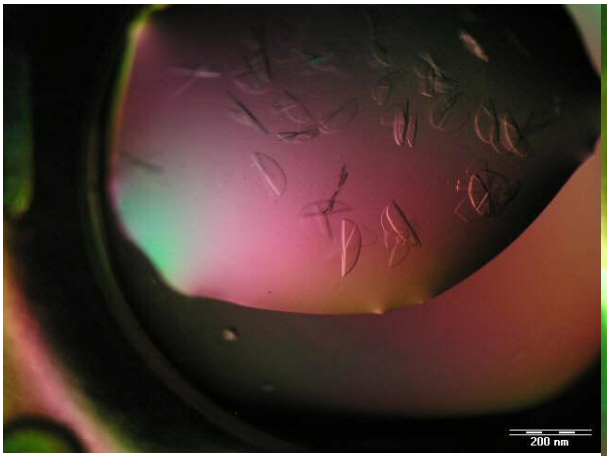

Figure 66 Initial crystals in Morpheus condition H10

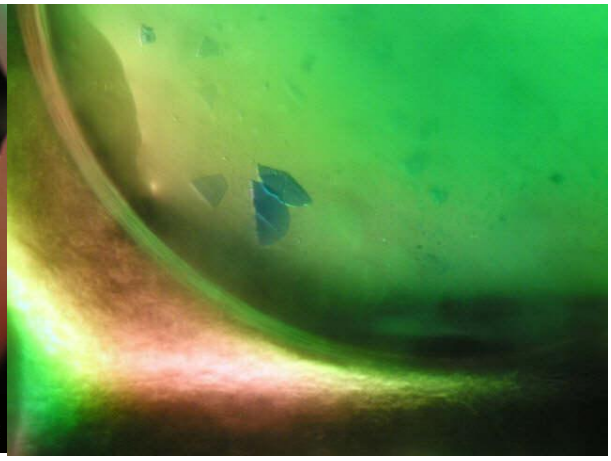

Figure 65 HctB crystals in Morpheus H10 stained with Izit dye

Initial crystals were obtained from a Morpheus screen in condition H10 (Figure 66). These crystals showed no diffraction, to determine if they were salt or protein they were stained with Izit dye (Figure 65). In order to get better crystals these initial crystals were used to make a micro seeding stock. New crystals were obtained in Morpheus H6 using micro seeding, unfortunately these crystals also did not diffract.

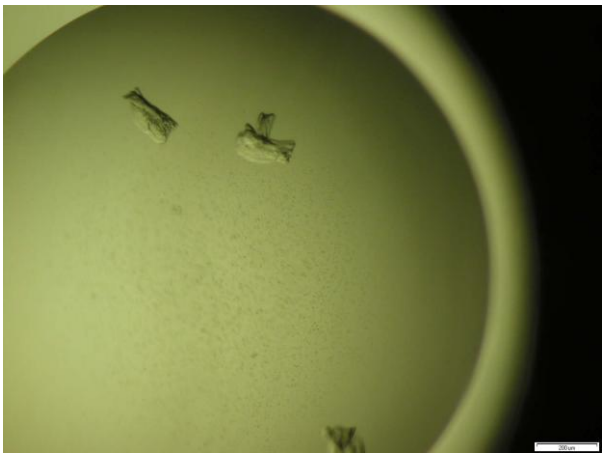

Figure 67 Crystals obtained in Morpheus H6 used microseeding

3.4 Discussion

So far it was not possible to obtain crystals showing protein diffraction. Therefore it is not entirely certain if the crystals obtained are protein crystals. The absence of salt diffraction can be considered a good sign since it means that the crystals do not consist of salt. Also the fact that staining the crystals with Izit dye (Figure 65) coloured them blue indicates that they include water channels. Additionally, seeding seems to work. These observations suggest that they are protein crystals. A possible reason why HctB crystal did not show any protein diffraction so far might be the platelet like nature of the crystals. Therefore growing thicker platelets or trying to obtain crystals with a different shape might solve the problem. Since all the crystals already appeared after 2 days growing them at lower temperature might be a good starting point for further crystallization trials.

4. References

1 **Enzyme Nomenclature. (1992) (Ed.: International Union of Biochemistry and Molecuar BIology). *Academic Press* New York**

2 **Turinsky J, O'Sullivan DM, Bayly BP (1990) 1,2-Diacylglycerol and ceramide levels in insulin-resistant tissues of the rat in vivo. *J Biol Chem* 265(28): 16880-16885**

3 **Itani SI, Ruderman NB, Schmieder F, Boden G (2002) Lipid-induced insulin resistance in human muscle is associated with changes in diacylglycerol, protein kinase C, and IkappaB-alpha. *Diabetes* 51(7): 2005-2011**

4 **Pilz S, Scharnagl H, Tiran B, Seelhorst U, Wellnitz B, Boehm BO, Schaefer JR, Marz W (2006) Free fatty acids are independently associated with all-cause and cardiovascular mortality in subjects with coronary artery disease. *J Clin Endocrinol Metab* 91(7): 2542-2547**

5 **Hotamisligil GS, Shargill NS, Spiegelman BM (1993) Adipose expression of tumor necrosis factor-alpha: direct role in obesity-linked insulin resistance. *Science* 259(5091): 87-91**

6 **Unger R.H., Clark G.O., Scherer P.E., Orci L. Lipid homeostasis, lipotoxicity and the metabolic syndrome. *Biochim Biophys Acta.* 2010;1801:209–214.**

7 **Slawik M., Vidal-Puig A.J. Lipotoxicity, overnutrition and energy metabolism in aging. *Ageing Res Rev.* 2006;5:144–164.**

8 **DeFronzo R.A. Dysfunctional fat cells, lipotoxicity and type 2 diabetes. *Int J Clin Pract Suppl.* 2004:9–21.**

9 **Lelliott C., Vidal-Puig A.J. Lipotoxicity, an imbalance between lipogenesis de novo and fatty acid oxidation. *Int J Obes Relat Metab Disord*. 2004;28(Suppl. 4):S22–S28.**

10 **Haemmerle G., Lass A., Zimmermann R., Gorkiewicz G., Meyer C., Rozman J. Defective lipolysis and altered energy metabolism in mice lacking adipose triglyceride lipase. *Science*. 2006;312:734–737.**

11 **Jenkins CM, Mancuso DJ, Yan W, Sims HF, Gibson B, Gross RW (2004) Identification, cloning, expression, and purification of three novel human calcium-independent phospholipase A2 family members possessing triacylglycerol lipase and acylglycerol transacylase activities. *J Biol Chem* 279(47): 48968-48975**

12 **Zechner, R., J. G. Strauss, G. Haemmerle, A. Lass, and R. Zimmermann. 2005. Lipolysis: pathway under construction. *Curr. Opin. Lipidol*. 16: 333–340. Medline**

13 **Rydel TJ, Williams JM, Krieger E, Moshiri F, Stallings WC, Brown SM, Pershing JC, Purcell JP, Alibhai MF (2003) The crystal structure, mutagenesis, and activity studies reveal that patatin is a lipid acyl hydrolase with a Ser-Asp catalytic dyad. *Biochemistry* 42(22): 6696-6708**

14 Lass A, Zimmermann R, Haemmerle G, Riederer M, Schoiswohl G, Schweiger M, Kienesberger P, Strauss JG, Gorkiewicz G, Zechner R (2006) Adipose triglyceride lipase-mediated lipolysis of cellular fat stores is activated by CGI-58 and defective in Chanarin-Dorfman Syndrome. *Cell Metab* 3(5): 309-319

15 Yang X, Lu X, Lombes M, Rha GB, Chi YI, Guerin TM, Smart EJ, Liu J (2010) The G(0)/G(1) switch gene 2 regulates adipose lipolysis through association with adipose triglyceride lipase. *Cell Metab* 11(3): 194-205

16 Vagin, AA, Steiner, RS, Lebedev, AA, Potterton, L, McNicholas, S, Long, F and Murshudov, GN. *Acta Cryst.* 2004 D60: 2284-2295

17 Yeaman, S. J. 1990. Hormone-sensitive lipase a multipurpose enzyme in lipid metabolism. *Biochim. Biophys. Acta*.

18 Stralfors, P., and P. Belfrage. 1983. Phosphorylation of hormone-sensitive lipase by cyclic AMP-dependent protein kinase. *J. Biol. Chem.*

19 Miyoshi, H., S. C. Souza, H. H. Zhang, K. J. Strissel, M. A. Christoffolete, J. Kovsan, A. Rudich, F. B. Kraemer, A. C. Bianco, M. S. Obin, et al. 2006. Perilipin promotes hormone-sensitive lipase-mediated adipocyte lipolysis via phosphorylation-dependent and -independent mechanisms. *J. Biol. Chem*. 281: 15837–15844

20 Sztalryd, C., G. Xu, H. Dorward, J. T. Tansey, J. A. Contreras, A. R. Kimmel, and C. Londos. 2003. Perilipin A is essential for the translocation of hormone-sensitive lipase during lipolytic activation. *J. Cell Biol.* 161: 1093–1103.

21 Zimmermann, R., J. G. Strauss, G. Haemmerle, G. Schoiswohl, R. Birner-Gruenberger, M. Riederer, A. Lass, G. Neuberger, F. Eisenhaber, A. Hermetter, et al. 2004. Fat mobilization in adipose tissue is promoted by adipose triglyceride lipase. *Science*. 306: 1383–1386

22 Harada, K., *W. J. Shen, S. Patel, V. Natu, J. Wang, J. Osuga, S. Ishibashi, and F. B. Kraemer.* 2003. *Resistance to high-fat diet-induced obesity and altered expression of adipose-specific genes in HSL-deficient mice. Am. J. Physiol. Endocrinol. Metab*. 285: E1182–*E1195*

23 Torben Østerlund, Douglas J. Beussman, Karin Julenius, Pak H. Poon, Sara Linse, Jeffrey Shabanowitz, Donald F. Hunt, Michael C. Schotz, Zygmunt S. Derewenda and Cecilia Holm. 1999. Domain Identification of Hormone-sensitive Lipase by Circular Dichroism and Fluorescence Spectroscopy, Limited Proteolysis, and Mass Spectrometry. *The Journal of Biological Chemistry*, 274, 15382-15388.

24 Tornqvist H, Belfrage P (1976) Purification and some properties of a monoacylglycerol-hydrolyzing enzyme of rat adipose tissue. *J Biol Chem* 251(3): 813-819

25 **T. P. Dinh, D. Carpenter, F. M. Leslie, T. F. Freund, I. Katona, S. L. Sensi, S. Kathuria, and D. Piomelli (2002) Brain monoglyceride lipase participating in endocannabinoid inactivation. *Proc Natl Acad Sci U S A*. 2002 August 6; 99(16): 10819–10824**

26 **Ulrike Taschler, Franz P. W. Radner, Christoph Heier, Renate Schreiber, Martina Schweiger, Gabriele Schoiswohl, Karina Preiss-Landl, Doris Jaeger, Birgit Reiter, Harald C. Koefeler, Jacek Wojciechowski, Christian Theussl, Josef M. Penninger, Achim Lass, Guenter Haemmerle, Rudolf Zechner, and Robert Zimmermann (2011) Monoglyceride Lipase Deficiency in Mice Impairs Lipolysis and Attenuates Diet-induced Insulin Resistance. *J Biol Chem*. 2011 May 20; 286(20): 17467–17477.**

27 **Bergsson G, Steingrimsson O, Thormar H (2002) Bactericidal effects of fatty acids and monoglycerides on Helicobacter pylori. *Int J Antimicrob Agents* 20(4): 258-262**

28 **Conley AJ, Kabara JJ (1973) Antimicrobial action of esters of polyhydric alcohols. *Antimicrob Agents Chemother* 4(5): 501-506**

29 **Kabara JJ, Vrable R (1977) Antimicrobial lipids: natural and synthetic fatty acids and monoglycerides. *Lipids* 12(9): 753-759**

30 **Thormar H, Hilmarsson H (2007) The role of microbicidal lipids in host defense against pathogens and their potential as therapeutic agents. *Chem Phys Lipids* 150(1)**

31 **Rengachari S, Bezerra GA, Riegler-Berket L, Gruber CC, Sturm C, Taschler U, Boeszoermenyi A, Dreveny I, Zimmermann R, Gruber K, Oberer M. (2012) The structure of monoacylglycerol lipase from Bacillus sp. H257 reveals unexpected conservation of the cap architecture between bacterial and human enzymes. *Biochim Biophys Acta.* 2012 Jul;1821(7):1012-21**

32 **Christoph Heier, Ulrike Taschler, Srinivasan Rengachari, Monika Oberer, Heimo Wolinski, Klaus Natter, Sepp D. Kohlwein, Regina Leber, and Robert Zimmermann (2010) Identification of Yju3p as functional orthologue of mammalian monoglyceride lipase in the yeast *Saccharomycescerevisiae. Biochim Biophys Acta.* 2010 September; 1801(9): 1063–1071**

33 **Muccioli GG, Sia A, Muchowski PJ, Stella N (2009) Genetic manipulation of palmitoylethanolamide production and inactivation in Saccharomyces cerevisiae. *PLoS One* 4(6): e5942**

34 **D.K. Nomura, J.Z. Long, S. Niessen, H.S. Hoover, S.W. Ng, B.F. Cravatt, Monoacylglycerol lipase regulates a fatty acid network that promotes cancer pathogenesis. Cell, 140 (2010), pp. 49–61**

35 **L. Ye, B. Zhang, E.G. Seviour, K.X. Tao, X.H. Liu, Y. Ling, J.Y. Chen, G.B. Wang, Monoacylglycerol lipase (MAGL) knockdown inhibits tumor cells growth in colorectal cancer. *Cancer Lett*., 307 (2011), pp. 6–17**

36 **Imamura S, Kitaura S (2000) Purification and characterization of a monoacylglycerol lipase from the moderately thermophilic Bacillus sp. H-257. *J Biochem* 127(3): 419-425**

37 **Casida JE, Quistad GB (2005) Serine hydrolase targets of organophosphorus toxicants. *Chem Biol Interact*** 157-158: **277-283**

38 **Aishwarya V. Ramaswamy, Carla M. Sorrels and William H. Gerwick, Cloning and Biochemical Characterization of the Hectochlorin Biosynthetic Gene Cluster from the Marine Cyanobacterium Lyngbya majuscula*. J. Nat. Prod.*, 2007, 70 (12), pp 1977–1986**

39 **Brian L. Marquez , Karl Shawn Watts , Alexandre Yokochi , Mary Ann Roberts , Pascal Verdier-Pinard , Jorge I. Jimenez , Ernest Hamel , Paul J. Scheuer , William H. Gerwick. Structure and Absolute Stereochemistry of Hectochlorin, a Potent Stimulator of Actin Assembly. *J. Nat. Prod.*, 2002, 65 (6), pp 866–871**

40 **Hendrik Luesch , Wesley Y. Yoshida , Richard E. Moore , Valerie J. Paul , Susan L. Mooberry. Isolation, Structure Determination, and Biological Activity of Lyngbyabellin A from the Marine Cyanobacterium Lyngbya majuscule. *J. Nat. Prod*., 2000, 63 (5), pp 611–615**

41 **Hampel A, Labanauskas M, Connors PG, et al. Single crystals of transfer RNA from formylmethionine and phenylalanine transfer RNAs. *Science* 1968;162:1384–7.**

42 **Ducruix, A. and Giege, R. (1992) Crystallization of nucleic acids and proteins. A practical approach, Oxford University Press, New York.**

43 **http://www.bruker-axs.de/fileadmin/user_upload/xrfintro/sec1_3.html**

44 **http://www.psi.ch/media/synchrotronquelle-sls**

45 **http://laue.web.psi.ch/laue-principle.htm 26.09.2012**

46 **Céline Schalk-Hihi, Carsten Schubert, Richard Alexander, Shariff Bayoumy, Jose C Clemente, Ingrid Deckman, Renee L DesJarlais, Keli C Dzordzorme, Christopher M Flores, Bruce Grasberger, James K Kranz, Frank Lewandowski, Li Liu, Hongchang Ma, Diane Maguire, Mark J Macielag, Mark E McDonnell, Tara Mezzasalma Haarlander, Robyn Miller, Cindy Milligan, Charles Reynolds, and Lawrence C Kuo. Crystal structure of a soluble form of human monoglyceride lipase in complex with an inhibitor at 1.35 Å resolution. *Protein Sci.* 2011 April; 20(4): 670–683.**

47 **http://www.embl.de/pepcore/pepcore_services/cloning/cloning_methods/chemically_competent/ 26.11.2012**

5. Appendix

5.1. Sequences

bMG LI145G mutant

```
bMGL-originalgene      ------------------------------ATGGGCAGCAGCCATCATCATCATCATCA 29
pET28a-bMGLI145G       ATTTTGTTTAACTTTAAGAAGGAGATATACCATGGGCAGCAGCCATCATCATCATCATCA 60
                                                      ****************************

bMGL-originalgene      CAGCAGCGGCCTGGTGCCGCGCGGCAGCCATATGAGCGAACAATATCCGGTGCTCTCGGG 89
pET28a-bMGLI145G       CAGCAGCGGCCTGGTGCCGCGCGGCAGCCATATGAGCGAACAATATCCGGTGCTCTCGGG 120
                       ************************************************************

bMGL-originalgene      CGCCGAGCCGTTTTACGCCGAAAACGGGCCGGTCGGGGTGCTGCTCGTGCACGGATTCAC 149
pET28a-bMGLI145G       CGCCGAGCCGTTTTACGCCGAAAACGGGCCGGTCGGGGTGCTGCTCGTGCACGGATTCAC 180
                       ************************************************************

bMGL-originalgene      CGGCACGCCCCACAGCATGCGCCCGCTCGCTGAAGCGTATGCGAAAGCCGGCTATACCGT 209
pET28a-bMGLI145G       CGGCACGCCCCACAGCATGCGCCCGCTCGCTGAAGCGTATGCGAAAGCCGGCTATACCGT 240
                       ************************************************************

bMGL-originalgene      TTGCCTGCCGCGCTTAAAAGGGCACGGAACGCATTACGAAGACATGGAACGGACGACGTT 269
pET28a-bMGLI145G       TTGCCTGCCGCGCTTAAAAGGGCACGGAACGCATTACGAAGACATGGAACGGACGACGTT 300
                       ************************************************************

bMGL-originalgene      CCACGATTGGGTCGCCTCGGTCGAAGAAGGATATGGATGGCTGAAACAACGATGCCAAAC 329
pET28a-bMGLI145G       CCACGATTGGGTCGCCTCGGTCGAAGAAGGATATGGATGGCTGAAACAACGATGCCAAAC 360
                       ************************************************************

bMGL-originalgene      CATTTTTGTCACCGGGCTGTCGATGGGCGGGACGCTCACGCTTTATTTGGCGGAACATCA 389
pET28a-bMGLI145G       CATTTTTGTCACCGGGCTGTCGATGGGCGGGACGCTCACGCTTTATTTGGCGGAACATCA 420
                       ************************************************************

bMGL-originalgene      CCCAGACATCTGCGGCATCGTGCCGATTAACGCCGCTGTCGACATCCCGGCCATCGCCGC 449
pET28a-bMGLI145G       CCCAGACATCTGCGGCATCGTGCCGATTAACGCCGCTGTCGACATCCCGGCCATCGCCGC 480
                       ************************************************************

bMGL-originalgene      CGGGATGACGGGCGGGGGCGAGCTGCCGAGGTATCTGGATTCGATCGGTTCGGACTTGAA 509
pET28a-bMGLI145G       CGGGATGACGGGCGGGGGCGAGCTGCCGAGGTATCTGGATTCGGGCGGTTCGGACTTGAA 540
                       ******************************************. ***************

bMGL-originalgene      AAATCCGGATGTGAAAGAGCTGGCATACGAGAAAACGCCGACCGCTTCGCTTCTTCAGCT 569
pET28a-bMGLI145G       AAATCCGGATGTGAAAGAGCTGGCATACGAGAAAACGCCGACCGCTTCGCTTCTTCAGCT 600
                       ************************************************************

bMGL-originalgene      GGCTAGGCTGATGGCACAGACAAAAGCGAAACTCGATCGCATCGTCTGTCCGGCGTTGAT 629
pET28a-bMGLI145G       GGCTAGGCTGATGGCACAGACAAAAGCGAAACTCGATCGCATCGTCTGTCCGGCGTTGAT 660
                       ************************************************************

bMGL-originalgene      TTTTGTCTCCGACGAAGATCACGTCGTGCCGCCGGGAAACGCCGACATCATCTTTCAAGG 689
pET28a-bMGLI145G       TTTTGTCTCCGACGAAGATCACGTCGTGCCGCCGGGAAACGCCGACATCATCTTTCAAGG 720
                       ************************************************************

bMGL-originalgene      CATTTCATCGACGGAGAAAGAGATCGTCCGCCTCCGAAACAGCTACCATGTGGCGACGCT 749
pET28a-bMGLI145G       CATTTCATCGACGGAGAAAGAGATCGTCCGCCTCCGAAACAGCTACCATGTGGCGACGCT 780
                       ************************************************************
```

```
bMGL-originalgene      CGATTACGACCAACCGATGATTATTGAACGGTCTCTCGAATTTTTCGCCAAGCACGCCGG 809
pET28a-bMGLI145G       CGATTACGACCAACCGATGATTATTGAACGGTCTCTCGAATTTTTCGCCAAGCACGCCGG 840
                       ************************************************************

bMGL-originalgene      ATAACTCGAG------------------------------------------------- 813
pET28a-bMGLI145G       ATAACTCGAGCACCACCACCACCACCACTGAGATCCGGCTGCTAACAAAGCCCGAAAGGA 900
                       **********
```

Histag sequence and linker region

NdeI site-CATATG; XhoI site-CTCGAG

Stop codon-TAA

Mutation: ATC to GGC

bMG LI145S mutant

```
bMGL-originalgene      ----------------------------ATGGGCAGCAGCCATCATCATCATCATCACA 31
pET28a-bMGLI145S       TTTGTTTAACTTTAAGAAGGAGATATACCATGGGCAGCAGCCATCATCATCATCATCACA 60
                                                    ******************************

bMGL-originalgene      GCAGCGGCCTGGTGCCGCGCGGCAGCCATATGAGCGAACAATATCCGGTGCTCTCGGGCG 91
pET28a-bMGLI145S       GCAGCGGCCTGGTGCCGCGCGGCAGCCATATGAGCGAACAATATCCGGTGCTCTCGGGCG 120
                       ************************************************************

bMGL-originalgene      CCGAGCCGTTTTACGCCGAAAACGGGCCGGTCGGGGTGCTGCTCGTGCACGGATTCACCG 151
pET28a-bMGLI145S       CCGAGCCGTTTTACGCCGAAAACGGGCCGGTCGGGGTGCTGCTCGTGCACGGATTCACCG 180
                       ************************************************************

bMGL-originalgene      GCACGCCCCACAGCATGCGCCCGCTCGCTGAAGCGTATGCGAAAGCCGGCTATACCGTTT 211
pET28a-bMGLI145S       GCACGCCCCACAGCATGCGCCCGCTCGCTGAAGCGTATGCGAAAGCCGGCTATACCGTTT 240
                       ************************************************************

bMGL-originalgene      GCCTGCCGCGCTTAAAAGGGCACGGAACGCATTACGAAGACATGGAACGGACGACGTTCC 271
pET28a-bMGLI145S       GCCTGCCGCGCTTAAAAGGGCACGGAACGCATTACGAAGACATGGAACGGACGACGTTCC 300
                       ************************************************************

bMGL-originalgene      ACGATTGGGTCGCCTCGGTCGAAGAAGGATATGGATGGCTGAAACAACGATGCCAAACCA 331
pET28a-bMGLI145S       ACGATTGGGTCGCCTCGGTCGAAGAAGGATATGGATGGCTGAAACAACGATGCCAAACCA 360
                       ************************************************************

bMGL-originalgene      TTTTTGTCACCGGGCTGTCGATGGGCGGGACGCTCACGCTTTATTTGGCGGAACATCACC 391
pET28a-bMGLI145S       TTTTTGTCACCGGGCTGTCGATGGGCGGGACGCTCACGCTTTATTTGGCGGAACATCACC 420
                       ************************************************************

bMGL-originalgene      CAGACATCTGCGGCATCGTGCCGATTAACGCCGCTGTCGACATCCCGGCCATCGCCGCCG 451
pET28a-bMGLI145S       CAGACATCTGCGGCATCGTGCCGATTAACGCCGCTGTCGACATCCCGGCCATCGCCGCCG 480
                       ************************************************************

bMGL-originalgene      GGATGACGGGCGGGGGCGAGCTGCCGAGGTATCTGGATTCGATCGGTTCGGACTTGAAAA 511
pET28a-bMGLI145S       GGATGACGGGCGGGGGCGAGCTGCCGAGGTATCTGGATTCGAGCGGTTCGGACTTGAAAA 540
                       ****************************************** *****************

bMGL-originalgene      ATCCGGATGTGAAAGAGCTGGCATACGAGAAAACGCCGACCGCTTCGCTTCTTCAGCTGG 571
pET28a-bMGLI145S       ATCCGGATGTGAAAGAGCTGGCATACGAGAAAACGCCGACCGCTTCGCTTCTTCAGCTGG 600
                       ************************************************************

bMGL-originalgene      CTAGGCTGATGGCACAGACAAAAGCGAAACTCGATCGCATCGTCTGTCCGGCGTTGATTT 631
pET28a-bMGLI145S       CTAGGCTGATGGCACAGACAAAAGCGAAACTCGATCGCATCGTCTGTCCGGCGTTGATTT 660
                       ************************************************************
```

```
bMGL-originalgene      TTGTCTCCGACGAAGATCACGTCGTGCCGCCGGGAAACGCCGACATCATCTTTCAAGGCA 691
pET28a-bMGLI145S       TTGTCTCCGACGAAGATCACGTCGTGCCGCCGGGAAACGCCGACATCATCTTTCAAGGCA 720
                       ************************************************************

bMGL-originalgene      TTTCATCGACGGAGAAAGAGATCGTCCGCCTCCGAAACAGCTACCATGTGGCGACGCTCG 751
pET28a-bMGLI145S       TTTCATCGACGGAGAAAGAGATCGTCCGCCTCCGAAACAGCTACCATGTGGCGACGCTCG 780
                       ************************************************************

bMGL-originalgene      ATTACGACCAACCGATGATTATTGAACGGTCTCTCGAATTTTTCGCCAAGCACGCCGGAT 811
pET28a-bMGLI145S       ATTACGACCAACCGATGATTATTGAACGGTCTCTCGAATTTTTCGCCAAGCACGCCGGAT 840
                       ************************************************************

bMGL-originalgene      AACTCGAG---------------------------------------------------- 813
pET28a-bMGLI145S       AACTCGAGCACCACCACCACCACCACTGAGATCCGGCTGCTAACAAAGCCCGAAAGGAAGC  900
                       ********
```

Histag sequence and linker region

NdeI site-CATATG; XhoI site-CTCGAG

Stop codon-TAA

Mutation: ATC to AGC

bMGLD196N mutant

```
bMGL-originalgene      ------------------------------------------------------------
pET28a-bMGLD196N       AGTATAGGGGAAAATTCCCCTCTAGAATAATTTTGTTTAACTTTAAGAAGGAGATATACC 60


bMGL-originalgene      ATGGGCAGCAGCCATCATCATCATCATCACAGCAGCGGCCTGGTGCCGCGCGGCAGCCAT 60
pET28a-bMGLD196N       ATGGGCAGCAGCCATCATCATCATCATCACAGCAGCGGCCTGGTGCCGCGCGGCAGCCAT 120
                       ************************************************************

bMGL-originalgene      ATGAGCGAACAATATCCGGTGCTCTCGGGCGCCGAGCCGTTTTACGCCGAAAACGGGCCG 120
pET28a-bMGLD196N       ATGAGCGAACAATATCCGGTGCTCTCGGGCGCCGAGCCGTTTTACGCCGAAAACGGGCCG 180
                       ************************************************************

bMGL-originalgene      GTCGGGGTGCTGCTCGTGCACGGATTCACCGGCACGCCCCACAGCATGCGCCCGCTCGCT 180
pET28a-bMGLD196N       GTCGGGGTGCTGCTCGTGCACGGATTCACCGGCACGCCCCACAGCATGCGCCCGCTCGCT 240
                       ************************************************************

bMGL-originalgene      GAAGCGTATGCGAAAGCCGGCTATACCGTTTGCCTGCCGCGCTTAAAAGGGCACGGAACG 240
pET28a-bMGLD196N       GAAGCGTATGCGAAAGCCGGCTATACCGTTTGCCTGCCGCGCTTAAAAGGGCACGGAACG 300
                       ************************************************************

bMGL-originalgene      CATTACGAAGACATGGAACGGACGACGTTCCACGATTGGGTCGCCTCGGTCGAAGAAGGA 300
pET28a-bMGLD196N       CATTACGAAGACATGGAACGGACGACGTTCCACGATTGGGTCGCCTCGGTCGAAGAAGGA 360
                       ************************************************************

bMGL-originalgene      TATGGATGGCTGAAACAACGATGCCAAACCATTTTTGTCACCGGGCTGTCGATGGGCGGG 360
pET28a-bMGLD196N       TATGGATGGCTGAAACAACGATGCCAAACCATTTTTGTCACCGGGCTGTCGATGGGCGGG 420
                       ************************************************************

bMGL-originalgene      ACGCTCACGCTTTATTTGGCGGAACATCACCCAGACATCTGCGGCATCGTGCCGATTAAC 420
pET28a-bMGLD196N       ACGCTCACGCTTTATTTGGCGGAACATCACCCAGACATCTGCGGCATCGTGCCGATTAAC 480
                       ************************************************************

bMGL-originalgene      GCCGCTGTCGACATCCCGGCCATCGCCGCCGGGATGACGGGCGGGGGCGAGCTGCCGAGG 480
pET28a-bMGLD196N       GCCGCTGTCGACATCCCGGCCATCGCCGCCGGGATGACGGGCGGGGGCGAGCTGCCGAGG 540
                       ************************************************************
```

```
bMGL-originalgene      TATCTGGATTCGATCGGTTCGGACTTGAAAAATCCGGATGTGAAAGAGCTGGCATACGAG 540
pET28a-bMGLD196N       TATCTGGATTCGATCGGTTCGGACTTGAAAAATCCGGATGTGAAAGAGCTGGCATACGAG 600
                       ************************************************************

bMGL-originalgene      AAAACGCCGACCGCTTCGCTTCTTCAGCTGGCTAGGCTGATGGCACAGACAAAAGCGAAA 600
pET28a-bMGLD196N       AAAACGCCGACCGCTTCGCTTCTTCAGCTGGCTAGGCTGATGGCACAGACAAAAGCGAAA 660
                       ************************************************************

bMGL-originalgene      CTCGATCGCATCGTCTGTCCGGCGTTGATTTTTGTCTCCGACGAAGATCACGTCGTGCCG 660
pET28a-bMGLD196N       CTCGATCGCATCGTCTGTCCGGCGTTGATTTTTGTCTCCGACGAAAATCACGTCGTGCCG 720
                       ********************************************.***************

bMGL-originalgene      CCGGGAAACGCCGACATCATCTTTCAAGGCATTTCATCGACGGAGAAAGAGATCGTCCGC 720
pET28a-bMGLD196N       CCGGGAAACGCCGACATCATCTTTCAAGGCATTTCATCGACGGAGAAAGAGATCGTCCGC 780
                       ************************************************************

bMGL-originalgene      CTCCGAAACAGCTACCATGTGGCGACGCTCGATTACGACCAACCGATGATTATTGAACGG 780
pET28a-bMGLD196N       CTCCGAAACAGCTACCATGTGGCGACGCTCGATTACGACCAACCGATGATTATTGAACGG 840
                       ************************************************************

bMGL-originalgene      TCTCTCGAATTTTTCGCCAAGCACGCCGGATAACTCGAG--------------------- 813
pET28a-bMGLD196N       TCTCTCGAATTTTTCGCCAAGCACGCCGGATAACTCGAGCACCACCACCACCACCACTGA 900

                       ****************************************
```

Histag sequence and linker region

NdeI site-CATATG; XhoI site-CTCGAG

Stop codon-TAA

Mutation: GAT to AAT

YJU3p L171S mutant

```
Yju3p-originalgene      ----ATGTCGTACTACCATCACCATCACCATCACGATTACGATATCCCAACGACCGAAAA 56
L171S_yju3.M13-24R      GCTTCAGTCG-TCTACCATCACCATCACCATCACGATTACGATATCCCAACGACCGAAAA 59
                            .:**** :************************************************

Yju3p-originalgene      CCTGTATTTTCAGGGCGCCATGGGATCCGCTCCGTATCCATACAAAGTGCAGACGACAGT 116
L171S_yju3.M13-24R      CCTGTATTTTCAGGGCGCCATGGGATCCGCTCCGTATCCATACAAAGTGCAGACGACAGT 119
                        ************************************************************

Yju3p-originalgene      ACCTGAACTTCAATACGAAAACTTTGATGGTGCTAAGTTCGGGTACATGTTCTGGCCTGT 176
L171S_yju3.M13-24R      ACCTGAACTTCAATACGAAAACTTTGATGGTGCTAAGTTCGGGTACATGTTCTGGCCTGT 179
                        ************************************************************

Yju3p-originalgene      TCAAAATGGCACCAATGAGGTCAGAGGTAGAGTTTTACTGATTCATGGGTTTGGCGAGTA 236
L171S_yju3.M13-24R      TCAAAATGGCACCAATGAGGTCAGAGGTAGAGTTTTACTGATTCATGGGTTTGGCGAGTA 239
                        ************************************************************

Yju3p-originalgene      CACAAAGATTCAATTCCGGCTTATGGACCACTTATCACTCAATGGTTACGAGTCATTTAC 296
L171S_yju3.M13-24R      CACAAAGATTCAATTCCGGCTTATGGACCACTTATCACTCAATGGTTACGAGTCATTTAC 299
                        ************************************************************

Yju3p-originalgene      GTTTGATCAAAGGGGTGCTGGTGTTACATCGCCGGGCAGATCGAAAGGTGTAACTGATGA 356
L171S_yju3.M13-24R      GTTTGATCAAAGGGGTGCTGGTGTTACATCGCCGGGCAGATCGAAAGGTGTAACTGATGA 359
                        ************************************************************
```

```
Yju3p-originalgene      GTACCATGTGTTTAACGATCTTGAGCATTTTGTGGAGAAGAACTTGAGTGAATGTAAGGC 416
L171S_yju3.M13-24R      GTACCATGTGTTTAACGATCTTGAGCATTTTGTGGAGAAGAACTTGAGTGAATGTAAGGC 419
                        ************************************************************
Yju3p-originalgene      CAAAGGCATACCCTTGTTCATGTGGGGGCATTCAATGGGCGGTGGTATCTGCCTAAACTA 476
L171S_yju3.M13-24R      CAAAGGCATACCCTTGTTCATGTGGGGGCATTCAATGGGCGGTGGTATCTGCCTAAACTA 479
                        ************************************************************
Yju3p-originalgene      TGCCTGCCAAGGTAAGCACAAAAACGAAATAAGCGGATATATCGGGTCAGGCCCATTAAT 536
L171S_yju3.M13-24R      TGCCTGCCAAGGTAAGCACAAAAACGAAATAAGCGGATATATCGGGTCAGGCCCATTAAT 539
                        ************************************************************
Yju3p-originalgene      AATTTTACATCCGCATACAATGTATAACAAGCCGACCCAAATTATTGCTCCATTATTGGC 596
L171S_yju3.M13-24R      AATTTTACATCCGCATACAATGTATAACAAGCCGACCCAAATTATTGCTCCATTATTGGC 599
                        ************************************************************
Yju3p-originalgene      GAAATTTTTACCAAGGGTAAGGATCGACACTGGTTTAGATCTTAAAGGAATCACATCTGA 656
L171S_yju3.M13-24R      GAAATTTTCACCAAGGGTAAGGATCGACACTGGTTTAGATCTTAAAGGAATCACATCTGA 659
                        ******** ***************************************************
Yju3p-originalgene      TAAAGCCTATCGTGCTTTCCTCGGAAGCGATCCTATGTCTGTTCCACTATATGGG-TCGT 715
L171S_yju3.M13-24R      TAAAGCCTATCGTGCTTTCCTCGGAAGCGATCCTATGTCTGTTCCACTATATGGGGTCGT 719
                        ******************************************************* ****
Yju3p-originalgene      TTAGGCAAATACACGACTTTATGCAACGTGGTGCCAAGCTCTACAAGAATGAAAACAATT 775
L171S_yju3.M13-24R      TTAGGCAAATACACGACTTTATGCAACGTGGTGCCAAGCTCTACAAGAATGAAAACAATT 779
                        ************************************************************
Yju3p-originalgene      ATATTCAGAAGAACTTCGCTAAAGACAAACCCGTTATTATTATGCATGGACAAGACGACA 835
L171S_yju3.M13-24R      ATATTCAGAAGAACTTCGCTAAAGACAAACCCGTTATTATTATGCATGGACAAGACGACA 839
                        ************************************************************
Yju3p-originalgene      CAATCAACGATCCTAAGGG-CTCTGAAAAGTTCATTCAGGACTGTCCTTCTGCTGACAAA 894
L171S_yju3.M13-24R      CAATCAACGATCCTAAAGGGCTCTGAAAAGTTCATTCGGGACTGTCCTTCTGCTGACAAA 899
                        ****************.** *****************.**********************
Yju3p-originalgene      GAATTAAAGCTGTATCCGGGCGCAAGACATTCGATTTTCTCACTAGAGACAGATAAAGTC 954
L171S_yju3.M13-24R      GAATTAAAGCTGTATCCCGGCGCAG-ACATTCGATTTTCTCACTAGAGACAGATAAAGTC 958
                        ***************** ******. **********************************
Yju3p-originalgene      TTCAACACGGTGTTCAATGATATGAAGCAATGGTTGGACAAACACACCACGACCGAAGCT 1014
L171S_yju3.M13-24R      TTCAACACGGTGTTCAATGATATGAAGCAATGGTTGGACAAACACACACG--ACGAAGCT 1016
                        ************************************************..   .*******
Yju3p-originalgene      AAACCATAA--------------------------------------------------- 1023
L171S_yju3.M13-24R      AAACCATAAGAATTCGAGCTCGTCGACAAGCTTGCGGCCGCACTCGAGGCATGCGGTACA 1076
                        *********
Yju3p-originalgene      ------------------------------------------------------------
L171S_yju3.M13-24R      AGCCTTGGCTGTTTTGGCGGAATGAGAGAGAAATTTTCATGCCCTTGATACAGATTAAAT 1136

Yju3p-originalgene      ------------------------------------------------------------
L171S_yju3.M13-24R      CAGAACGCAGAGCCGGCTGATAAACAGAAATATGTCCTTGGCGGCGAATAACAGCCGCGT 1196

Yju3p-originalgene      ---------------------------------------------
```

```
L171S_yju3.M13-24R      GTTACAACTTGGATCCATGCCGGATCTTCAAGTGAAGCCCGTAG 1240
```

Histag sequence and linker region
BamHI site-CATATG
Stop codon-TAA
Mutation: TTA to TCA